AIMS Mathematics, 7(11): 19696–19726.
DOI: 10.3934/math.20221080
Received: 23 June 2022
Revised: 11 August 2022
Accepted: 22 August 2022
Published: 06 September 2022

http://www.aimspress.com/journal/Math

Research article

A variational image denoising model under mixed Cauchy and Gaussian noise

Miyoun Jung*

Department of Mathematics, Hankuk University of Foreign Studies, Yongin 17035, Korea

* **Correspondence:** Email: mjung@hufs.ac.kr; Tel: +82313304261.

Abstract: In this article, we propose a novel variational model for restoring images in the presence of the mixture of Cauchy and Gaussian noise. The model involves a novel data-fidelity term that features the mixed noise as an infimal convolution of two noise distributions and total variation regularization. This data-fidelity term contributes to suitable separation of Cauchy noise and Gaussian noise components, facilitating simultaneous removal of the mixed noise. Besides, the total variation regularization enables adequate denoising in homogeneous regions while conserving edges. Despite the nonconvexity of the model, the existence of a solution is proven. By employing an alternating minimization approach and the alternating direction method of multipliers, we present an iterative algorithm for solving the proposed model. Experimental results validate the effectiveness of the proposed model compared to other existing models according to both visual quality and some image quality measurements.

Keywords: image denoising; mixed Cauchy-Gaussian noise; variational model; infimal convolution; total variation
Mathematics Subject Classification: 68U10, 65K10, 94A08, 49J40

1. Introduction

Different image acquisition and transmission factors cause the observed images corrupted by a mixture of noise statistics. Image denoising aims to retrieve a clean image from the observed noisy image, which is an essential problem in image processing. We here focus on the image denoising problem in the presence of mixed Cauchy and additive white Gaussian noise. In real circumstances, there are noises with a strong impulsive nature which the Gaussian model fails to describe, such as atmospheric noise caused by lighting, picture noise, radar noise and so on. The Cauchy noise is a type of alpha-stable noise that is impulsive in nature and has a heavy tail. It can occur in low-frequency atmospheric signals [1], underwater acoustic signals [2, 3], radar clutter [4, 5], multiple access

interference in wireless communication systems [6], powerline communication channels [7], air turbulence [8], biomedical images, and synthetic aperture radar images [9, 10]. Thus, the removal of Cauchy noise has been of great importance in many applications such as sonar, radar, image processing and communications [11–13]. On the other hand, the additive white Gaussian noise frequently appears due to the temperature of the sensor and the level of illumination in the environment that corrupts every pixels. These noises can appear simultaneously in practice. Indeed, the mixed Cauchy and Gaussian noise can occur in real world applications such as communication systems, where in the receiver one has the sum of the Gaussian noise due to electronic components and impulsive noise due to environmental effects [14], or astrophysical image processing [15], where the cosmic microwave background radiation is described as the sum of Gaussian distributed from the antenna beam and symmetric alpha-stable distributed random variables from galaxies. Thus, it is a necessary problem to suppress this mixed noise.

Let $\Omega \subset \mathbb{R}^2$ be a connected bounded image domain with a Lipschitz boundary. We consider a noisy image $f : \Omega \to \mathbb{R}$ given by

$$f = u + n, \tag{1.1}$$

where n is the mixture of Cauchy noise and Gaussian noise. The Gaussian noise is assumed to follow a Gaussian distribution, $\mathcal{N}(0, \sigma^2)$, with zero mean and standard deviation σ, and the Cauchy noise is assumed to follow a Cauchy distribution, $C(0, \gamma)$. Specifically, the Cauchy noise, w, is a random variable following a Cauchy distribution, denoted by $C(\delta, \gamma)$, with the probability density function (PDF) [16, 17]

$$P(w; \delta, \gamma) = \frac{\gamma}{\pi\Big((w-\delta)^2 + \gamma^2\Big)}, \tag{1.2}$$

where $\delta \in \mathbb{R}$ is the parameter representing the location of the peak, and $\gamma > 0$ is the scale parameter that determines the level of noise. The Cauchy distribution looks similar to a Gaussian distribution with a bell-shaped curve, but it is a heavy-tailed distribution, as shown in Figure 1(a). Its tail heaviness is determined by the parameter γ, and it increases as the value of γ increases, which can be seen in Figure 1(b). Owing to the tail heaviness, the Cauchy distribution is more prone to producing values that fall far from its mean. Hence, the noise generated from the Cauchy distribution is more impulsive than the Gaussian one. For instance, the Cauchy noise tends to contain much larger noise spikes than the Gaussian noise. In this work, we intend to recover a clean image u from the noisy image f, which is an ill-posed inverse problem.

To solve the ill-posed inverse problem (1.1), one of the well-known approaches is to solve a minimization problem of the following form:

$$\min_u \; E(u) = \Phi(u, f) + R(u), \tag{1.3}$$

where Φ is a data-fidelity term that depends on the type of noise, and R is a regularization term that controls the smoothness of u. The most popular regularization is the total variation (TV) [18], due to its convexity and edge preserving property. Many TV based variational models have been proposed for restoring images with various types of noise, such as Gaussian noise [18], impulse noise [19–21], multiplicative noise [22–25], Poisson noise [26], Rician noise [27, 28], and Cauchy noise [29–31]. The

different noise distributions yield different data-fidelity terms, so one can attain suitable variational image denoising models depending on noise types. For instance, the L^2 data-fidelity term, $\Phi(u, f) = \int_\Omega (f-u)^2\, dx$, is typically used for the image denoising models under Gaussian noise [18], and $\Phi(u, f) = \int_\Omega |f - u|\, dx$ is more appropriate for the ones under impluse noise [19].

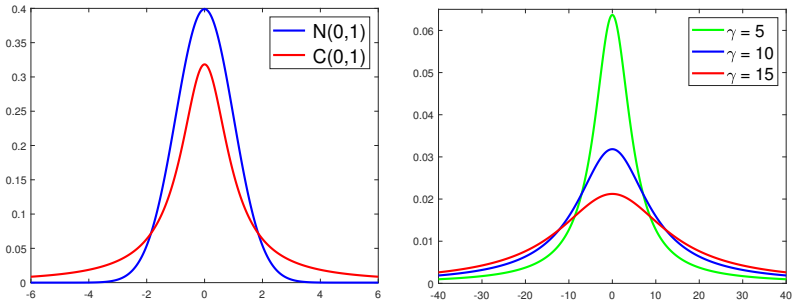

(a) (b)

Figure 1. Comparison of Cauchy distribution $C(0, \gamma)$ and Gaussian distribution $\mathcal{N}(0, \sigma^2)$. (a) PDFs of $C(0, 1)$ (red) and $\mathcal{N}(0, 1)$ (blue), (b) PDFs of $C(0, \gamma)$ with $\gamma = 5$ (green), $\gamma = 10$ (blue), $\gamma = 15$ (red).

While there are numerous denoising methods for Gaussian noise, several approaches to eliminate Cauchy noise have been suggested. In addition to the Markov random field or wavelet-based denoising methods [32–34], a TV-based model was proposed in [29], with the nonconvex data-fidelity term derived from the Cauchy distribution (1.2). The same authors also suggested a convex model by inserting a quadratic penalty term that involves a pre-denoised image achieved by applying the median filtering to the noisy data. However, the median filtering does not always yield satisfactory denoising results. In [30], Mei et al. showed the effectiveness of the nonconvex model in [29] combined with the nonconvex alternating direction method of multipliers (ADMM) [35]. Moreover, a convex TV model was proposed in [31] for restoring images with α-stable noise with $\alpha \in (0, 2)$ (Cauchy noise when $\alpha = 1$, Gaussian noise when $\alpha = 2$). The experimental results showed that the model outperformed the L^1-TV [36] and Cauchy [29] models in impulsive noisy environments (i.e., $\alpha \in (0, 1.5)$), while providing comparable performance in less impulsive noisy environments (i.e., $\alpha \in (1.5, 2)$). The aforementioned nonconvex or convex TV models in [29] have also been extended in various works [37–43] by adopting other regularization terms instead of TV.

Removing the mixture of noise is more challenging because of the unique nature of each of two types of noise. For the removal of mixed impulse and Gaussian noise, various efficient two-phase methods that integrate variational methods with adaptive median filters have been proposed [44–46]. These two-phase approaches strongly rely on precise detection of noisy pixels. A unified framework of joint detection of noisy pixels and reduction of noise components has been suggested in [47–49]. Moreover, the combination of data-fidelity terms has been considered. Specifically, a linear combination of the L^1 and L^2 data-fidelity terms was considered [50, 51]. The removal of mixed Poisson and Gaussian (MPG) has also been extensively studied. Some early works are based on the noise parameter estimation [52, 53], while others are mainly based on transform-domain procedures [54–58], such as variance-stabilizing transformation [59] or Haar wavelet transform. The MAP approaches [60, 61] lead to practical difficulties since the log-likelihood function involves

infinite summation. The combination of data-fidelity terms has also been considered for MPG removal [61–64]. In [65, 66], the authors proposed new TV-based denoising models under the mixed salt-and-pepper and Gaussian noise or MPG noise, by utilizing a data discrepancy which characterizes the mixed noise as an infimal convolution of two noise distributions. These data-fidelity terms provided better denoising performance than a combination of different data-fidelity terms corresponding to noise types. In [67], new operator-splitting algorithms were suggested for solving the MPG model in [65]. On the other hand, there are a few works for dealing with mixed Cauchy and Gaussian noise, and they are only for 1D signals [14, 15, 68, 69]. In this work, we introduce a new model for restoring images under mixed Cauchy and Gaussian noise, by following the idea of the work [65, 66].

To the best of our knowledge, there is no unified model for simultaneously removing both Cauchy and Gaussian noise from images, so our main contribution is to propose a novel model for denoising images with the mixed noise. In spite of the nonconvexity of the proposed model, the existence of a solution is proved. We also present an efficient iterative optimization algorithm. The rest of the paper is organized as follows. Section 2 recalls some variational models for restoring images with Cauchy noise. In Section 3, we propose a minimization problem for image denoising under mixed noise, along with an optimization algorithm for solving the proposed model. Section 4 presents experimental results with comparisons to other existing models, and Section 5 concludes our work with some comments.

2. Variational models for Cauchy noise removal

Assuming that the Cauchy noise follows a zero-centered Cauchy law ($\delta = 0$), Sciacchitano et al. [29] derived a TV based model for the removal of Cauchy noise:

$$\min_{u\in BV(\Omega)} \lambda \int_\Omega \log(\gamma^2 + (f-u)^2)\, dx + \int_\Omega |Du|, \tag{2.1}$$

where $\mathrm{BV}(\Omega)$ is the subspace of functions $u \in L^1(\Omega)$ such that the following BV semi-norm is finite [18]:

$$\int_\Omega |Du| := \sup_{\phi\in C_c^1(\Omega,\mathbb{R}^2),\, \|\phi\|_\infty \le 1} \int_\Omega u \,\mathrm{div}(\phi)\, dx, \tag{2.2}$$

where the vector measure Du represents the distributional or weak gradient of u, and $\|\cdot\|_\infty$ is the essential supremum norm. This is also called the total variation of u, denoted by $\mathrm{TV}(u)$. If $u \in w^{1,1}(\Omega)$, then $\int_\Omega |Du| = \int_\Omega |\nabla u|\, dx$. $\lambda > 0$ is a tuning parameter that determines the smoothness of the restored image u. Despite the nonconvexity of the model (2.1), the existence and uniqueness of a minimizer was proved under certian conditions. Mei et al. [30] also showed the efficiency of the model (2.1) associated with the alternating direction method of multipliers (ADMM) [35].

Recently, Yang et al. [31] proposed a convex TV model for restoring images degenerated by the α-stable noise ($0 < \alpha < 2$), including Cauchy noise ($\alpha = 1$):

$$\min_{u\in BV(\Omega)} \lambda \Big(\int_\Omega \log\left(\gamma + |f-u|\right)\, dx + \frac{\mu}{2}\|u-g\|_2^2 \Big) + \int_\Omega |Du|, \tag{2.3}$$

where $\mu > 0$ is a parameter, and g is the pre-denoised image obtained by applying a median filter to f. The existence and uniqueness of a minimizer for the model (2.3) was shown, and the model was

efficiently solved by employing the primal-dual algorithm [70]. The numerical results showed that the model (2.3) provided better denoising performance than the existing models [20, 29], especially when the noise has more impulsive properties (i.e., $\alpha \in (0, 1.5)$).

3. Description of the proposed model and algorithm

3.1. Proposed model and convergence analysis

In this section, we introduce a new image denoising model in the presence of the mixture of Cauchy noise and Gaussian noise.

In general, both Cauchy noise and Gaussian noise are additive noise, so we assume that both noises occur simultaneously and independently in the entire domain. Thus, we consider a noisy image $f \in L^2(\Omega)$ given by

$$f = u + w + v, \tag{3.1}$$

where w is the Cauchy noise following the Cauchy distribution $C(0, \gamma)$, and v is the Gaussian noise following the Gaussian distribution $\mathcal{N}(0, \sigma^2)$. Since w and v occur independently, the order of w and v does not matter.

To eliminate both Gaussian noise v and Cauchy noise $w = f - u - v$ from the data f, we follow the idea in [65] which suggested infimal convolution-type data-fidelity terms for the dismissal of mixed SP-Gaussian noise or mixed Poisson-Gaussian noise. Now we define an infimal convolution-type data-fidelity term to remove mixed Cauchy and Gaussian noise as

$$\Phi(u, f) := \inf_{v \in L^2(\Omega)} \Big\{ \lambda_1 \Phi_1(v) + \lambda_2 \Phi_2(u, f - v) \Big\}, \tag{3.2}$$

where Φ_1 and Φ_2 are the Gaussian and Cauchy noise components, respectively, defined as

$$\begin{aligned} \Phi_1(v) &= \|v\|_2^2, \\ \Phi_2(u, f - v) &= \int_\Omega \log(\gamma^2 + (f - u - v)^2)\, dx, \end{aligned} \tag{3.3}$$

where Φ_2 is acquired from the data-fidelity term in (2.1), which is nonconvex. λ_1 and λ_2 are positive parameters that balances the smoothing effect of the regularization as well as the fitting with respect to the intensity of each single noise distribution in f.

By integrating the data-fidelity term in (3.2) with the TV regularization, we propose the following minimization problem for restoring images with mixed Cauchy and Gaussian noise:

$$\min_{u \in X,\, v \in L^2(\Omega)} \Big\{ \mathcal{E}(u, v) = \lambda_1 \Phi_1(v) + \lambda_2 \Phi_2(u, f - v) + \int_\Omega |Du| + \frac{\mu}{2} \|u - g\|_2^2 \Big\}, \tag{3.4}$$

where $X = BV(\Omega) \cap L^2(\Omega)$, g is the pre-denoised image by applying a median filter to the data f, and $\mu > 0$ is a parameter. The median filtering does not always bring adequate denoising results, but we add the last quadratic term mainly for the proof of the existence of a minimizer. Indeed, we in practice set the value of μ very small so that the pre-denoised image g barely impacts on the denoising results. We note that the proposed model can be extended, by utilizing other regularization terms, instead of

TV, such as the higher-order regularization [71, 72], nonlocal TV [73], dictionary learning [74, 75], or tight-frame approach [76], etc. This work mainly focuses on introducing a new data-fidelity term for the mixed Cauchy-Gaussian noise model, so the adoption of new regularization terms are beyond the scope of our work.

The energy functional $\mathcal{E}$ in (3.4) is nonconvex without any specific assumptions on the parameters, but it is still available to show the existence of a minimizer for the minimization problem (3.4). In the following theorem, we prove the existence of a minimizer for the problem (3.4).

Theorem 1. *Let $f \in L^2(\Omega)$, and $g \in L^2(\Omega)$. Then, the minimization problem (3.4) has at least one solution $(u^*, v^*) \in X \times L^2(\Omega)$ with $X = BV(\Omega) \cap L^2(\Omega)$.*

Proof. Since Φ_2 has the minimum value $2|\Omega| \log \gamma$ when $u + v = f$, the functional E in (3.4) is bounded from below. Then we can choose a minimizing sequence (u_n, v_n) in $X \times L^2(\Omega)$ such that $\mathcal{E}(u_n, v_n) \leq C$ for a constant $C > 0$. So all terms in $\mathcal{E}(u_n, v_n)$ are bounded, i.e.,

$$\begin{aligned} &\|v_n\|_2^2 \leq C, \quad \int_\Omega \log(\gamma^2 + (f - u_n - v_n)^2)\, dx \leq C, \\ &\|u_n - g\|_2^2 \leq C, \quad \int_\Omega |Du_n| \leq C. \end{aligned} \tag{3.5}$$

Hence we can extract a subsequence $\{v_n\}$ (still denoted in the same way) weakly converging to v^* in $L^2(\Omega)$ and $v_n \to v^*$ a.e. in Ω. Then we have that

$$\|v^*\|_2^2 \;\leq\; \liminf_{n\to\infty} \|v_n\|_2^2. \tag{3.6}$$

Since $g \in L^2(\Omega)$, $\{u_n\}$ is bounded in $L^2(\Omega)$ from (3.5) and thus bounded in $L^1(\Omega)$. Besides, $\{\int_\Omega |Du_n|\}$ is bounded, so $\{u_n\}$ is bounded in $BV(\Omega)$. Hence, there is a subsequence $\{u_n\}$ (still denoted in the same way) and u^* in $BV(\Omega)$ such that (i) $u_n \to u^*$ strongly in $L^1(\Omega)$, (ii) $u_n \rightharpoonup u^*$ weakly in $L^2(\Omega)$, (iii) $u_n \to u^*$ in a.e. Ω, and (iv)

$$\int_\Omega |Du^*| \leq \liminf_{n\to\infty} \int_\Omega |Du_n|. \tag{3.7}$$

Lastly, from Fatou's Lemma, we can finally attain that

$$\mathcal{E}(u^*, v^*) \leq \liminf_{n\to\infty} \mathcal{E}(u_n, v_n), \tag{3.8}$$

which indicates that (u^*, v^*) is a minimzer of $\mathcal{E}(u, v)$. □

Remark. The functional $\mathcal{E}$ in (3.4) is convex under certain conditions. Specifically, it can be easily proven that $\mathcal{E}(u, \cdot)$ is strictly convex if $\lambda_2 \leq 4\gamma^2\mu$, while $\mathcal{E}(\cdot, v)$ is strictly convex if $\lambda_2 \leq 8\gamma^2\lambda_1$. Furthermore, if $\lambda_2 < \frac{1}{2}\min\{8\gamma^2\lambda_1, 4\gamma^2\mu\}$, then $\mathcal{E}(u, v)$ is strictly convex (for the proof, see Appendix A), so it has a unique minimizer. However, we in practice do not impose this condition on the parameter λ_2 due to the following reason: we want to reduce the influence of the pre-denoised image g, so we set the value of μ to be very small. This leads to a small value of λ_2 with the aforementioned condition, but a small value of λ_2 is not appropriate for the removal of Cauchy noise especially when the level of Cauchy noise is high. Therefore, without the above constraint on λ_2, the functional $\mathcal{E}$ is nonconvex, hence we practically solve the nonconvex minimization problem.

3.2. Optimization algorithm

To solve the proposed model (3.4), we consider a discretized image domain $\Omega = \{(i, j) : i = 1, 2, ..., M, j = 1, 2, ..., N\}$, and let u_s be the pixel value of an image u at location $s \in \Omega$. Then we compute numerically the solution pair of the following minimization problem:

$$\begin{aligned} &\min_{u,v} \left\{\lambda_1\|v\|_2^2 + \lambda_2\, G(u, v) + \|\nabla u\|_1 + \frac{\mu}{2}\|u - g\|_2^2\right\} \\ &\text{with} \quad G(u, v) = \langle \log(\gamma^2 + (f - u - v)^2), \mathbf{1}\rangle, \end{aligned} \tag{3.9}$$

where $\langle\ ,\ \rangle$ is the inner product, $\|\cdot\|_2^2 = \langle\cdot, \cdot\rangle$, and $\|\nabla u\|_1$ is the discrete version of the isotropic TV norm:

$$\|\nabla u\|_1 = \sum_s \sqrt{\left(\partial_{x_1} u\right)_s^2 + \left(\partial_{x_2} u\right)_s^2},$$

with $\nabla u = [\partial_{x_1} u, \partial_{x_2} u]^T$, denoting $\partial_{x_1} u$ and $\partial_{x_2} u$ by the finite difference operators that estimate the partial derivatives of the image u along the x_1-axis and x_2-axis, respectively.

To solve the nonconvex problem (3.9), we first adopt the alternating minimization algorithm (AMA). The AMA minimizes a function of two variables, and its essential idea is to keep one variable fixed while minimizing the other variable and iterate this process. This approach has practically performed well, even though the objective function is nonconvex. The AMA applied to (3.9) yields the following iterative algorithm:

$$\begin{aligned} u^{k+1} &\in \arg\min_u \left\{\lambda_2\, G(u, v^k) + \|\nabla u\|_1 + \frac{\mu}{2}\|u - g\|_2^2\right\}, \\ v^{k+1} &\in \arg\min_v \left\{\lambda_1\|v\|_2^2 + \lambda_2\, G(u^{k+1}, v)\right\}. \end{aligned} \tag{3.10}$$

In the subsequent paragraphs, we solve the two subproblems in (3.10).

3.2.1. Solving the u-subprolem in (3.10)

First, to solve the u-subproblem in (3.10), we adopt the alternating direction method of multipliers (ADMM) [35] applied to nonconvex minimization problems with linear constraints. By introducing an auxiliary variable z, we can rewrite the u-subproblem in (3.10) as the following equivalent constrained problem:

$$\begin{aligned} &\min_{u,z} \left\{\lambda_2\, G(z, v^k) + \|\nabla u\|_1 + \frac{\mu}{2}\|u - g\|_2^2\right\}, \\ &\text{subject to:} \quad z = u. \end{aligned} \tag{3.11}$$

Then the augmented Lagrangian function (ALF) corresponding to (3.11) is given by

$$\mathcal{L}_\tau(u, z, p) = \lambda_2\, G(z, v^k) + \|\nabla u\|_1 + \frac{\mu}{2}\|u - g\|_2^2 - \langle p, z - u\rangle + \frac{\tau}{2}\|z - u\|_2^2, \tag{3.12}$$

where $p \in \mathbb{R}^{M\times N}$ is the Lagrangian multiplier, and $\tau > 0$ is a penalty parameter.

The ADMM applied to (3.11) leads to the following iterative algorithm:

$$\begin{cases} u^{\ell+1} \in \arg\min_u \ \mathcal{L}_\tau(u, z^\ell, p^\ell), \\ z^{\ell+1} \in \arg\min_z \ \mathcal{L}_\tau(u^{\ell+1}, z, p^\ell), \\ p^{\ell+1} = p^\ell + \tau(u^{\ell+1} - z^{\ell+1}). \end{cases} \tag{3.13}$$

Following the Theorem 4.2 in [30], we can prove a convergence of the ADMM in (3.13) as follows:

Theorem 2. *If $\tau > \frac{2\lambda_2}{\gamma^2} - \mu$, then the sequence $\{(u^\ell, z^\ell, p^\ell)\}$ generated by the algorithm (3.13) converges globally to a point (u^*, z^*, p^*), which is a stationary point of $\mathcal{L}_\tau$.*

The proof of this theorem is omitted since it is similar to the proof given in [30]. The stationary point (u^*, z^*, p^*) satisfies the Karush–Kuhn–Tucker (KKT) conditions of problem (3.11). However, the minimization problem (3.11) is non-convex, so the KKT conditions are only necessary optimal conditions to (3.11). Hence, we cannot assure that (u^*, z^*) is an optimal solution of (3.11).

In the following paragraphs, we solve the two subproblems in (3.13).

***u*-subproblem in (3.13).** First, the u-subproblem in (3.13) is convex, so it can be efficiently solved by various convex optimization algorithms [70, 77–80]. Among them, we again utilize the ADMM [79, 80]. Specifically, to handle the nondifferential L^1 term, we introduce an auxiliary variable $\vec{d}$ to replace ∇u, and then achieve the following constrained problem:

$$\begin{aligned} &\min_{u,\vec{d}} \ \|\vec{d}\|_1 + \frac{\mu}{2}\|u - g\|_2^2 - \langle p^\ell, z^\ell - u\rangle + \frac{\tau}{2}\|z^\ell - u\|_2^2, \\ &\text{subject to:} \quad \vec{d} = \nabla u. \end{aligned} \tag{3.14}$$

Analogously, the ALF for the problem (3.14) is

$$\mathcal{L}_\eta(u, \vec{d}, \vec{q}) = \|\vec{d}\|_1 + \frac{\mu}{2}\|u - g\|_2^2 - \langle p^\ell, z^\ell - u\rangle + \frac{\tau}{2}\|z^\ell - u\|_2^2 - \langle \vec{q}, \vec{d} - \nabla u\rangle + \frac{\eta}{2}\|\vec{d} - \nabla u\|_2^2, \tag{3.15}$$

where $\vec{q} \in (\mathbb{R}^{M\times N})^2$ is the vector of Lagrangian multipliers, and $\eta > 0$ is a penalty parameter. Then the ADMM algorithm applied to (3.14) results in the following iterative algorithm:

$$\begin{cases} u^{m+1} \in \arg\min_u \ \mathcal{L}_\eta(u, \vec{d}^m, \vec{q}^m), \\ \vec{d}^{m+1} \in \arg\min_{\vec{d}} \ \mathcal{L}_\eta(u^{m+1}, \vec{d}, \vec{q}^m), \\ \vec{q}^{m+1} = \vec{q}^m + \eta(\nabla u^{m+1} - \vec{d}^{m+1}). \end{cases} \tag{3.16}$$

Algorithm 1 Solving the proposed model (3.4).

Input: choose the parameters λ_1, λ_2, μ, τ, $\eta > 0$, the maximum iteration numbers N_u, N_{uu}, N_z.
Initialization: set $u^0 = \max(\min(f, 255), 0)$, $v^0 = 0$, $z^0 = u^0$, $p^0 = 0$, $\vec{q}^0 = \mathbf{0}$.
repeat
  Compute u^{k+1} by iterating for $\ell = 0, 1, 2, \cdots, N_u$:
    compute $u^{\ell+1}$ by iterating for $m = 0, 1, 2, \cdots, N_{uu}$:
      u^{m+1} by solving (3.17) using DCT,
      $\vec{d}^{m+1} = shrink\left(\nabla u^{m+1} + \frac{\vec{q}^m}{\eta}, \frac{1}{\eta}\right)$,
      $\vec{q}^{m+1} = \vec{q}^m + \eta(\nabla u^{m+1} - \vec{d}^{m+1})$.
    compute $z^{\ell+1}$ by iterating for $n = 0, 1, 2, \cdots, N_z$:
      $z^{n+1} = z^n - \tau\frac{F'(z^n)}{F''(z^n)}$,
    update $p^{\ell+1} = p^\ell + \tau(u^{\ell+1} - z^{\ell+1})$.
  Compute v^{k+1} by solving Eq (3.25) using Cardano's formula.
until a stopping condition is satisfied.
Output: restored image u.

The u-subproblem in (3.16) is a least squares problem, so the solution u^{m+1} in (3.16) can be attained by solving the following normal equation:

$$(\mu + \tau + \eta\nabla^T\nabla)u = \mu g + \tau(z^\ell - p^\ell/\tau) + \eta\nabla^T(\vec{d}^m - \vec{q}^m/\eta), \tag{3.17}$$

where $\nabla^T = -div$ with a discrete divergence opterator such that $div(w_1, w_2) = \partial_{x_1}w_1 + \partial_{x_2}w_2$. In discrete setting, $\nabla^T\nabla$ is equal to $-\Delta$, where Δ is a discrete Laplacian operator. The discrete Laplacian operator can be regarded as the convolution of the kernel [0 1 0; 1 −4 1; 0 1 0]. Then, since Δ is a symmetric convolution operator, $\mu + \tau + \eta\nabla^T\nabla$ can be diagonalized by the 2-dimensional discrete cosine transform (DCT2) under the symmetric boundary condition [81]. Thus we solve the Eq (3.17) using the DCT2, denoted by $\mathcal{F}$, under the symmetric boundary condition. Then we can obtain an explicit formula for u^{m+1}:

$$u^{m+1} = \mathcal{F}^{-1}\left(\frac{\mathcal{F}(\mu g + \tau(z^\ell - p^\ell/\tau) + \eta\nabla^T(\vec{d}^m - \vec{q}^m/\eta))}{\mu + \tau + \eta\mathcal{F}(\nabla^T\nabla)}\right), \tag{3.18}$$

where $\mathcal{F}^{-1}$ denotes the inverse DCT2.

Lastly, the solution $\vec{d}^{m+1}$ in (3.16) can be explicitly obtained as

$$\vec{d}^{m+1} = shrink\left(\nabla u^{m+1} + \frac{\vec{q}^m}{\eta}, \frac{1}{\eta}\right), \tag{3.19}$$

where *shrink* is the soft thresholding operator defined as

$$shrink(t, \xi)_s = \frac{t_s}{|t_s|} \cdot \max(|t_s| - \xi, 0), \tag{3.20}$$

where $|t_s| = \sqrt{(t_{1,s})^2 + (t_{2,s})^2}$ with $t = [t_1, t_2]^T$.

z-subproblem in (3.13). Next we solve the z-subproblem in (3.13), which can be rewritten as

$$\min_{z} \ \lambda_2\langle\log(\gamma^2 + (z + v^k - f)^2), \mathbf{1}\rangle + \frac{\tau}{2}\|z - u^{\ell+1} - p^\ell/\tau\|_2^2. \tag{3.21}$$

The first-order optimality condition for $z^{\ell+1}$ is given by

$$F'(z) = 2\lambda_2\frac{z + v^k - f}{\gamma^2 + (z + v^k - f)^2} + \tau(z - u^{\ell+1} - p^\ell/\tau) = 0, \tag{3.22}$$

where $F(z) = \lambda_2\log(\gamma^2 + (z + v^k - f)^2) + \frac{\tau}{2}(z - u^{\ell+1} - p^\ell/\tau)^2$. This normal Eq (3.22) can be efficiently solved by using Newton's method as follows:

$$z^{n+1} = z^n - \frac{F'(z^n)}{F''(z^n)}. \tag{3.23}$$

The z-subproblem (3.21) is strictly convex if $\lambda_2 \leq 4\gamma^2\tau$. This condition is satisfied in practice, so Eq (3.22) has a unique real root. Hence, with a good initial guess, Newton's method converges fast within a few number of iterations. Meanwhile, Eq (3.22) can be rewritten as a cubic equation by multiplying with the denominator. This cubic equation can be explicitly solved using Cardano's formula [82]. In our simulations, we decide to utilize Newton's method due to its efficiency. Indeed, despite the same denoising results, the total computational time when using Newton's method is shorter than when using Cardano's formula.

3.2.2. Solving the v-subprolem in (3.10)

Lastly, we solve the v-subproblem in the AMA (3.10):

$$\min_{v} \ \lambda_1\|v\|_2^2 + \lambda_2\,\langle\log(\gamma^2 + (v + u^{k+1} - f)^2), \mathbf{1}\rangle. \tag{3.24}$$

The necessary optimality condition for v^{k+1} is

$$\lambda_1 v + \lambda_2\frac{v + u^{k+1} - f}{\gamma^2 + (v + u^{k+1} - f)^2} = 0. \tag{3.25}$$

The problem (3.24) is convex if $\lambda_2 \leq 8\gamma^2\lambda_1$. In practice, this condition is not satisfied due to the choice of small values for λ_1. Thus, the problem (3.24) is not convex, so we utilize the Cardano's formula to solve Eq (3.25). Specifically, Eq (3.25) can be written as the following cubic equation:

$$av^3 + bv^2 + cv + d = 0, \tag{3.26}$$

with $a = \lambda_1$, $b = 2\lambda_1(u^{k+1} - f)$, $c = \lambda_1(\gamma^2 + (u^{k+1} - f)^2) + \lambda_2$, $d = \lambda_2(u^{k+1} - f)$. The Cardano's formula for real roots of a cubic polynomial is given in the following proposition [82].

Proposition 1. *For the cubic equation with real coefficients*

$$ax^3 + bx^2 + cx + d = 0, \quad a \neq 0, \tag{3.27}$$

define $Q = \frac{3ac-b^2}{9a^2}$, $R = \frac{9abc-27a^2d-2b^3}{54a^3}$, *and the discriminant* $D = Q^3 + R^2$. *If* $D > 0$, *the cubic equation (3.27) has only one real root, which is given by*

$$x = \sqrt[3]{R + \sqrt{D}} + \sqrt[3]{R - \sqrt{D}} - \frac{b}{3a}. \tag{3.28}$$

Otherwise, if $D \leq 0$, *Eq (3.27) has three real roots (possibly equal), which are given by*

$$x = 2\sqrt{-Q}\cos\Big(\frac{\theta + 2k\pi}{3}\Big) - \frac{b}{3a}, \quad k = 0, 1, 2, \tag{3.29}$$

where $\theta = \cos^{-1}(R/\sqrt{-Q^3})$.

If the Eq (3.25) has three real roots, we choose one which yields the minimum value of the objective function in (3.24).

Consequently, the whole algorithm for solving the problem (3.9) is given in Algorithm 1.

4. Experimental results

This section presents the experimental results of the proposed model (3.4) and comparisons to other existing models. We compare our model with two Cauchy denoising models, nonconvex TV model (Cauchy-TV) [29, 30] and Yang et al.'s model [31] (Yang's), given in (2.1) and (2.3), respectively. Furthermore, due to the impulsive characteristics of Cauchy noise, we also present the denoising results of the median filtering (MF) [83] and L^1-TV model [19]. For solving the L^1-TV and Cauchy-TV models, we employ the convex or nonconvex ADMM algorithms.

4.1. Experimental setting

The test images are given in Figure 2, and the size of images are 256×256 or 481×321. The range of intensity values in original images is assumed to be $[0, 255]$. The Cauchy noise w is generated by applying the following property: If X and Y are two independent Gaussian distributed random variables with mean 0 and variance 1, then the ratio X/Y follows the standard Cauchy distribution, i.e., $C(0, 1)$ [84, 85]. Thus $w = \gamma\frac{n_1}{n_2}$, where n_1 and n_2 follow the standard normal distribution, $\mathcal{N}(0, 1)$, independently. In the experiments, we consider the four mixed noise cases: $(\gamma, \sigma) = (10, 20)$, $(10, 30)$, $(15, 10)$, $(15, 20)$. In the Yang's model (2.3), the parameter γ is set to be the exact Cauchy noise level like our model.

Figure 2. Original clean images. Top to bottom (left to right): Barbara, Bird, Boat, Building (481×321), Cameraman, Castle (481×321), Lake, Lena, Parrot, Peppers, Pirate, Policemen (481×321).

The quality of restored images is measured by the Peak-Signal-to-Noise-Ratio (PSNR) value as

$$\text{PSNR}(u, u_*) = 10 \log_{10}\Big(\frac{255^2 MN}{\|u - u_*\|_2^2}\Big), \tag{4.1}$$

where u and u_* are the restored and original images respectively. We also compute the structural similarity index measure (SSIM) [86], which is a perception-based measure that uses information about the structure of the objects in the visual sense. Specifically, we compute the mean SSIM index value between two images u and u_* using

$$\text{SSIM}(\mathbf{x}, \mathbf{y}) = \frac{(2\mu_{\mathbf{x}}\mu_{\mathbf{y}} + c_1)(2\sigma_{\mathbf{xy}} + c_2)}{(\mu_{\mathbf{x}}^2 + \mu_{\mathbf{y}}^2 + c_1)(\sigma_{\mathbf{x}}^2 + \sigma_{\mathbf{y}}^2 + c_2)}, \tag{4.2}$$

where $\mathbf{x}$ and $\mathbf{y}$ are the spatial patches extracted from u and u_* respectively, $\mu_{\mathbf{x}}$ and $\sigma_{\mathbf{x}}^2$ represent the average and variance of $\mathbf{x}$ respectively, and c_1 and c_2 are some constants for stability. For a noisy data f, the intensity values of some noisy pixels are much larger (or smaller) than 255 (or 0) and they mainly affect the PSNR value of f, so the PSNR of f cannot be properly computed. Thus, we compute the PSNR value of the cropped image, $\max(\min(f, 255), 0)$, instead of f, which are given in Tables 1–4. Moreover, we use this cropped image as an initial condition for u from the experiments in [30].

Table 1. Denoising results with mixed Cauchy-Gaussian noise when $(\gamma, \sigma) = (10, 20)$.

Model	u^0 (cropped f)		Median filter		Cauchy-TV [30]		L^1-TV [19]		Yang et al. [31]		Proposed	
Image	PSNR	SSIM	PSNR	SSIM	PSNR	SSIM	PSNR	SSIM	PSNR	SSIM	PSNR	SSIM
barbara	15.41	0.2557	22.34	0.5333	23.77	0.6410	23.92	0.6488	23.90	0.6573	**24.33**	**0.6741**
bird	15.53	0.1354	28.53	0.7056	29.89	0.8610	30.02	0.8693	30.18	0.8736	**30.49**	**0.8786**
boat	15.41	0.2693	22.41	0.5136	23.67	0.6057	23.79	0.6118	23.94	0.6193	**24.39**	**0.6373**
building	15.45	0.2461	22.75	0.5817	23.77	0.6984	23.80	0.7068	24.10	0.7179	**24.52**	**0.7378**
cameraman	15.53	0.2181	22.85	0.5831	24.68	0.7377	24.75	0.7395	24.87	0.7506	**25.50**	**0.7756**
castle	15.41	0.1820	23.36	0.5876	25.00	0.7442	25.11	0.7502	25.14	0.7560	**25.84**	**0.7777**
lake	15.33	0.3048	22.10	0.5793	23.28	0.6725	23.29	0.6772	23.31	0.6764	**24.13**	**0.7150**
lena	15.39	0.2183	24.95	0.6421	25.91	0.7211	26.01	0.7240	26.26	0.7368	**26.45**	**0.7494**
parrot	15.39	0.2453	23.12	0.6435	24.91	0.7375	24.94	0.7375	25.21	0.7583	**25.51**	**0.7811**
peppers	15.40	0.2055	25.26	0.7033	26.15	0.7825	25.86	0.7790	26.36	0.7981	**26.92**	**0.8084**
pirate	15.43	0.2889	23.03	0.4892	23.83	0.5483	24.00	0.5634	24.03	0.5613	**24.31**	**0.5690**
policemen	15.40	0.2839	20.00	0.4963	21.61	0.6541	21.82	0.6712	21.82	0.6762	**22.47**	**0.7079**
Avergae	15.42	0.2377	23.29	0.5882	24.71	0.7003	24.77	0.7065	24.92	0.7151	**25.41**	**0.7343**

* Note: Bold values indicate the best denoising performance.

Table 2. Denoising results with mixed Cauchy-Gaussian noise when $(\gamma, \sigma) = (10, 30)$.

Model	u^0 (cropped f)		Median filter		Cauchy-TV [30]		L^1-TV [19]		Yang et al. [31]		Proposed	
Image	PSNR	SSIM	PSNR	SSIM	PSNR	SSIM	PSNR	SSIM	PSNR	SSIM	PSNR	SSIM
barbara	14.55	0.2193	21.53	0.4620	22.88	0.5732	23.19	0.5965	23.30	0.6100	**23.61**	**0.6238**
bird	14.62	0.1143	26.76	0.6129	28.16	0.8319	28.67	0.8459	28.73	**0.8544**	**29.12**	0.8471
boat	14.46	0.2293	21.98	0.4618	22.86	0.5510	23.21	0.5739	23.32	0.5779	**23.63**	**0.5972**
building	14.61	0.2145	22.22	0.5175	22.90	0.6487	23.21	0.6697	23.42	0.6803	**23.45**	**0.6874**
cameraman	14.62	0.1908	22.22	0.5097	23.70	0.7040	24.12	0.7033	24.32	0.7208	**24.66**	**0.7465**
castle	14.58	0.1603	22.71	0.5027	24.20	0.7069	24.56	0.7158	24.58	0.7280	**24.97**	**0.7399**
lake	14.63	0.2707	21.59	0.5313	22.49	0.6202	22.86	0.6461	22.91	0.6519	**23.35**	**0.6752**
lena	14.53	0.1889	24.09	0.5762	24.82	0.6754	25.12	0.6909	25.36	0.7066	**25.67**	**0.7100**
parrot	14.67	0.2231	22.48	0.5799	23.71	0.7106	24.12	0.7172	24.24	0.7434	**24.55**	**0.7482**
peppers	14.55	0.1783	24.14	0.6316	24.72	0.7373	24.77	0.7448	25.16	0.7667	**25.61**	**0.7655**
pirate	14.59	0.2489	22.42	0.4526	23.09	0.5029	23.31	0.5159	23.33	0.5062	**23.61**	**0.5283**
policemen	14.65	0.2576	19.72	0.4315	20.88	0.6118	21.28	0.6386	21.32	0.6448	**21.45**	**0.6564**
Average	14.58	0.2080	22.65	0.5224	23.70	0.6562	24.03	0.6715	24.16	0.6825	**24.47**	**0.6938**

* Note: Bold values indicate the best denoising performance.

Table 3. Denoising results with mixed Cauchy-Gaussian noise when $(\gamma, \sigma) = (15, 10)$.

Model	u^0 (cropped f)		Median filter		Cauchy-TV [30]		L^1-TV [19]		Yang et al. [31]		Proposed	
Image	PSNR	SSIM	PSNR	SSIM	PSNR	SSIM	PSNR	SSIM	PSNR	SSIM	PSNR	SSIM
barbara	14.61	0.2278	22.38	0.5471	24.06	0.6666	23.86	0.6517	23.95	0.6627	**24.13**	**0.6687**
bird	14.44	0.1150	28.98	0.7423	30.44	0.8736	30.17	0.8668	30.58	0.8792	**30.72**	**0.8800**
boat	14.49	0.2331	22.45	0.5289	24.31	0.6476	23.99	0.6318	23.89	0.6213	**24.42**	**0.6486**
building	14.51	0.2171	22.83	0.6055	24.27	0.7328	23.76	0.7120	23.99	0.7182	**24.31**	**0.7386**
cameraman	14.54	0.1914	23.05	0.6201	25.06	0.7684	24.76	0.7519	24.82	0.7647	**25.28**	**0.7761**
castle	14.47	0.1605	23.41	0.6129	25.58	0.7719	25.28	0.7504	25.13	0.7601	**25.83**	**0.7810**
lake	14.58	0.2785	22.14	0.6005	23.86	0.7082	23.51	0.6937	23.60	0.6965	**24.12**	**0.7204**
lena	14.53	0.1952	25.16	0.6629	26.35	0.7471	26.06	0.7339	26.22	0.7417	**26.52**	**0.7518**
parrot	14.48	0.2236	23.18	0.6741	25.34	0.7788	24.82	0.7674	25.18	0.7771	**25.57**	**0.7870**
peppers	14.46	0.1789	25.30	0.7296	26.77	0.7998	26.13	0.7763	26.36	0.8029	**26.97**	**0.8068**
pirate	14.48	0.2497	23.10	0.4990	24.23	0.5749	24.08	0.5715	23.95	0.5508	**24.36**	**0.5780**
policemen	14.47	0.2560	20.03	0.5213	21.88	0.6906	21.58	0.6757	21.55	0.6695	**22.05**	**0.7044**
Average	14.50	0.2105	23.50	0.6120	25.18	0.7300	24.83	0.7152	24.93	0.7203	**25.35**	**0.7367**

* Note: Bold values indicate the best denoising performance.

Table 4. Denoising results with mixed Cauchy-Gaussian noise when $(\gamma, \sigma) = (15, 20)$.

Model	u^0 (cropped f)		Median filter		Cauchy-TV [30]		L^1-TV [19]		Yang et al. [31]		Proposed	
Image	PSNR	SSIM	PSNR	SSIM	PSNR	SSIM	PSNR	SSIM	PSNR	SSIM	PSNR	SSIM
barbara	14.04	0.2053	21.63	0.4855	23.50	0.6235	23.42	0.6159	23.54	0.6304	**23.64**	**0.6315**
bird	14.16	0.1067	27.49	0.6569	29.16	0.8538	29.11	0.8532	29.25	0.8592	**29.49**	**0.8652**
boat	14.11	0.2205	22.21	0.4869	23.49	0.5958	23.43	0.5946	23.49	0.5984	**23.89**	**0.6119**
building	14.11	0.2024	22.41	0.5462	23.39	0.6877	23.36	0.6834	23.63	0.6959	**23.97**	**0.7126**
cameraman	14.09	0.1784	22.44	0.5448	24.35	0.7404	24.10	0.7343	24.31	0.7368	**24.76**	**0.7583**
castle	14.11	0.1498	22.94	0.5392	24.84	0.7416	24.71	0.7310	24.77	0.7385	**25.17**	**0.7561**
lake	14.18	0.2580	21.82	0.5581	23.18	0.6693	23.10	0.6644	23.17	0.6675	**23.48**	**0.6836**
lena	14.07	0.1771	24.47	0.6083	25.51	0.7159	25.36	0.7099	25.64	0.7199	**25.75**	**0.7255**
parrot	14.10	0.2087	22.71	0.6146	24.50	0.7413	24.24	0.7350	24.52	0.7543	**24.78**	**0.7643**
peppers	14.07	0.1682	24.55	0.6633	25.69	0.7672	25.06	0.7652	25.51	0.7818	**25.99**	**0.7862**
pirate	14.03	0.2259	22.59	0.4673	23.60	0.5405	23.56	0.5421	23.58	0.5337	**23.83**	**0.5436**
policemen	14.12	0.2446	19.84	0.4621	21.52	0.6560	21.36	0.6497	21.44	0.6565	**22.07**	**0.6860**
Average	14.09	0.1954	22.92	0.5527	24.39	0.6944	24.23	0.6898	24.40	0.6973	**24.74**	**0.7104**

* Note: Bold values indicate the best denoising performance.

The stopping criterion for our model is given by

$$\frac{\|g^{iter+1} - g^{iter}\|_2}{\|g^{iter+1}\|_2} < tol, \quad \text{or} \quad iter > MaxIter, \tag{4.3}$$

where $g = u$ or z, tol is a given tolerance, and $MaxIter$ is a maximum iteration number. For our model, we set $tol = 10^{-4}$. For the L^1-TV and Yang's models, we use the same stopping condition as ours, while for the Cauchy-TV model we use the stopping condition given in [30]. For our model, the maximum iteration number for Newton's method for z is fixed as $N_z = 5$, and we fix $N_u = 10$ and $N_{uu} = 5$.

The selection of parameters for our model is as follows: The parameter μ is fixed as 10^{-7}, and the penalty parameters τ and η in the ADMM algorithms are fixed as 1. The parameters λ_1 and λ_2 mainly influences on the quality of the restored images, and they are tuned to achieve the best denoising results. Indeed, the parameter λ_1 is set to be 0.05 when $(\gamma, \sigma) = (15, 10)$, and 0.02 for the other noise cases. The values of the parameter λ_2 are given in all figures.

4.2. Denoising results

First, Figure 3 compares noisy images and signals degraded by the Cauchy noise with $\gamma = 10$, Gaussian noise with $\sigma = 20$, mixed Cauchy and Gaussian noise with $(\gamma, \sigma) = (10, 20)$, respectively. The cross-sectional lines in the right column show that the vertical scale for the noisy signal corrupted by the Cauchy noise goes from -200 to 900, which shows the impulsive feature of the Cauchy noise. Besides, although the noisy signal distorted by the mixed noise is mainly influenced by the Cauchy noise, it can be seen that the Gaussian noise also further distorts the signal.

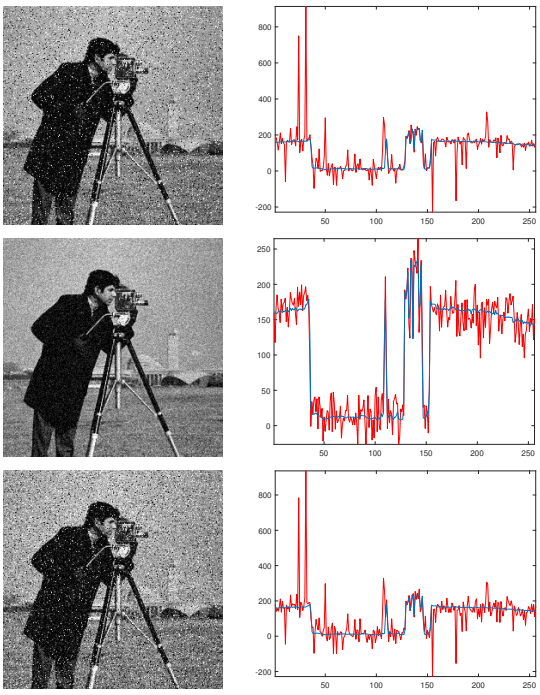

Figure 3. Noisy images (left) and their cross-sectional lines (right), degraded by (top row) Cauchy noise with $\gamma = 10$, (middle) Gaussian noise with $\sigma = 20$, (bottom) mixed Cauchy-Gaussian noise with $(\gamma, \sigma) = (10, 20)$. Blue line: Original clean signal, Red line: Noisy signal.

In Figure 4, we compare the denoising results of all models when the noise level is $(\gamma, \sigma) = (10, 20)$. The data images are given in Figure 5. First we can see that the MF enables to remove both noise to

some extent, but its restored images are noisier and blurrier than the ones using the other TV models. Among the TV models, the L^1-TV provides similar denoising results to the Cauchy-TV model. This is due to that the L^1 data-fidelity is suitable for eliminating both impulsive noise and Gaussian noise. On the other hand, the Yang's model supplies slightly better or similar denoising results than the L^1-TV model, which also explains the capability of the Yang's model to handle both noise. In fact, the Yang's model provides averagely higher PSNR and SSIM values than the L^1-TV model in all noise cases, as shown in Tables 1–4. Compared with these existing models, our model generates cleaner homogeneous regions, such as the sky areas in Boat and Cameraman, while better conserving textures and details, such as the textural part in Barbara, the ropes and iron pillars in Boat, the face and tripod parts in Cameraman. This can be more clearly seen in the zoomed images in Figure 6. Moreover, all these observations also match the highest PSNR and SSIM values of our model, as shown in Table 1. Overall, these examples justify the effectiveness of our data-fidelity term for getting rid of mixed Cauchy and Gaussian noise.

In Figure 7, we present the denoising results with higher Cauchy noise level and smaller Gaussian noise level, i.e., $(\gamma, \sigma) = (15, 10)$. Unlike the denoising results when $(\gamma, \sigma) = (10, 20)$, the Cauchy-TV model furnishes better denoising results than the L^1-TV and Yang's model. This implies that as the Cauchy noise level increases while the Gaussian noise level decreases, the performance of the Cauchy-TV model much enhances unlike the other models. In particular, the Yang's model retain some Cauchy noise in the restored images, which can be more obviously seen in the zoomed images in Figure 8. Indeed, this problem might be fixed by decreasing the regularization parameter λ or increasing the size of a median filter applied to g, but these cause much smoother restored images with much less PSNR values. Thus we choose these given images as the best restored images of the Yang's model. Despite the improved performance of the Cauchy-TV model, our model provides better preserved details and cleaner smooth regions than the other models, which can be seen in the window parts in Castle and sky areas in Policemen. These also lead to the highest PSNR values of our model. These also show the outstanding performance of our model over the other models. Lastly, Figure 9 presents the final Gaussian components, v, corresponding to the final restored images, u, given in 7. This validates that our model properly separates the Gaussian and Cauchy noise components.

Figure 10 compares the denoising results when $(\gamma, \sigma) = (10, 20), (10, 30), (15, 20)$. First, it can be observed that the Cauchy-TV model does not perform well in the presence of high-level of Gaussian noise, although it properly removes the Cauchy noise. Moreover, the Yang's model seems to deal with both noise to a certain degree, but it keeps some Cauchy noise under a high level of Cauchy noise, as shown in the denoised image when $(\gamma, \sigma) = (15, 20)$. The L^1-TV model moderately performs for deleting both noise, but its performance does not exceed the Yang's one with respect to the PSNR and SSIM values. In contrast, our model well eliminates both noise in all noise cases, by sufficiently denoising homogenous regions while conserving fine structures and edges than the other models.

In Figure 11, we present zoomed denoised images when $(\gamma, \sigma) = (10, 30)$ and $(\gamma, \sigma) = (15, 20)$, respectively. The zoomed data images are given in the first row. When $(\gamma, \sigma) = (10, 30)$, the denoised images of our model and Yang's model seem to be visually indistinguishable, but our model brings cleaner homogeneous regions, such as the sky areas in both examples. On the other hand, the Yang's model fails to adequately remove the Cauchy noise, whose trace can be detected in some pixels in the Pirate image. But our model sufficiently denoise smooth regions with better keeping delicate features than the other models, leading to the highest PSNR values. These can be observed in the eye area in

Parrot and face region in Pirate. Hence, our model attains more satisfactory denoising results even when the noise level of Cauchy or Gaussian noise is high.

In Tables 1–4, we report the PSNR and SSIM values of the restored images of all models. The proposed model yields the highest PSNR and SSIM values in almost all cases. Overall, our model leads to the best denoising results with regard to these image quality assessments. These also confirm the superior performance of our model over the existing models.

(a) Median filter (b) Cauchy-TV [30] (c) L^1-TV [19] (d) Yang et al. [31] (e) Proposed

Figure 4. Denoising results of our model and other models when $(\gamma, \sigma) = (10, 20)$. (a) median filter of size 4×4 (top row) or 5×5 (middle-bottom rows). PSNR values (left to right): (top row) 22.34/23.77/23.92/23.90/24.33, (middle) 22.41/23.67/23.79/23.94/24.39, (bottom) 22.85/24.68/24.75/24.87/25.50. Parameter λ_2 of the proposed model (top to bottom): 24, 23, 23.

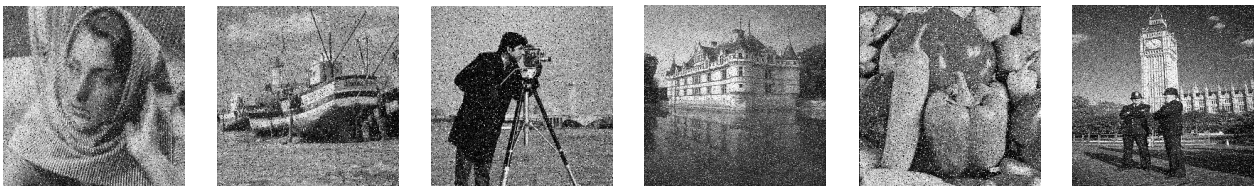

Figure 5. Noisy data f. 1st-3rd columns: Mixed Cauchy-Gaussian noise with $(\gamma, \sigma) = (10, 20)$, 4th-6th columns: Mixed Cauchy-Gaussian noise with $(\gamma, \sigma) = (15, 10)$.

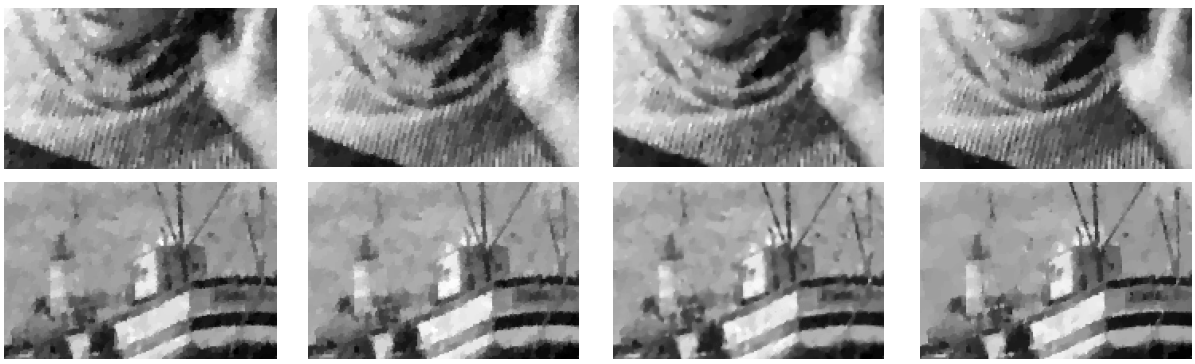

(a) Cauchy-TV [30] (b) L^1-TV [19] (c) Yang et al. [31] (d) Proposed

Figure 6. Zoomed denoised images from Figure 4.

(a) Median filter (b) Cauchy-TV [30] (c) L^1-TV [19] (d) Yang et al. [31] (e) Proposed

Figure 7. Denoising results of our model and other models when $(\gamma, \sigma) = (15, 10)$. (a) median filter of size 5×5. PSNR values (left to right): (top row) 23.41/25.58/25.28/25.13/25.83, (middle) 25.30/26.77/26.13/26.36/26.97, (bottom) 20.03/21.88/21.58/21.55/22.05. Parameter λ_2 of the proposed model (top to bottom): 29, 30, 30.

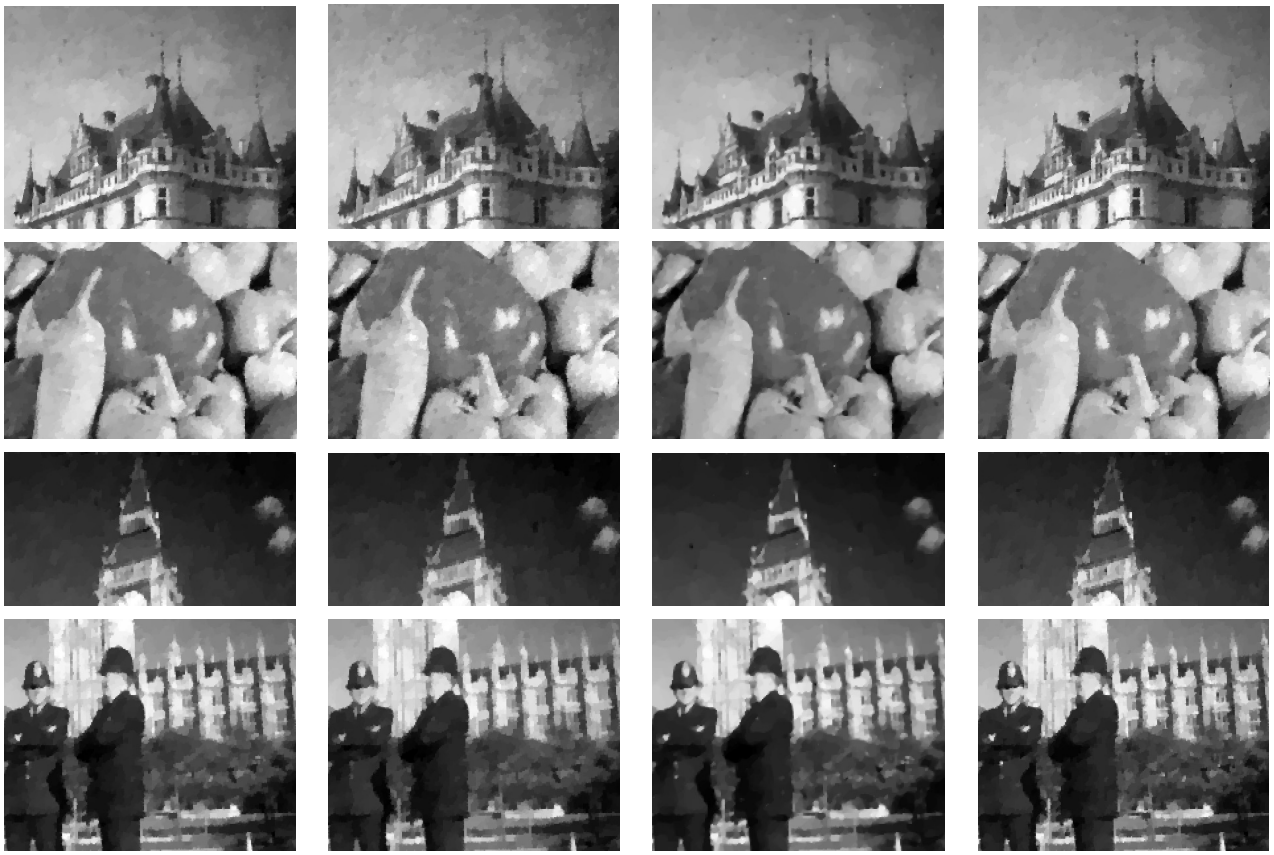

(a) Cauchy-TV [30] (b) L^1-TV [19] (c) Yang et al. [31] (d) Proposed

Figure 8. Zoomed denoised images from Figure 7.

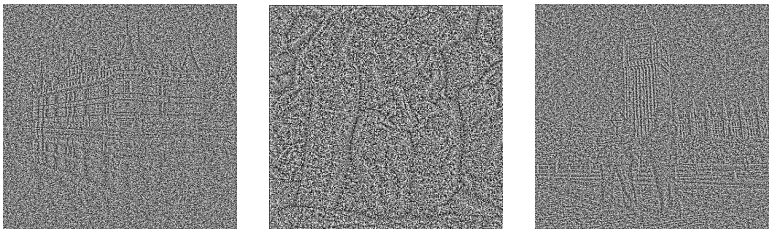

Figure 9. Final Gaussian noise components v corresponding to the denoised images u of the proposed model in Figure 7 when $(\gamma, \sigma) = (15, 10)$.

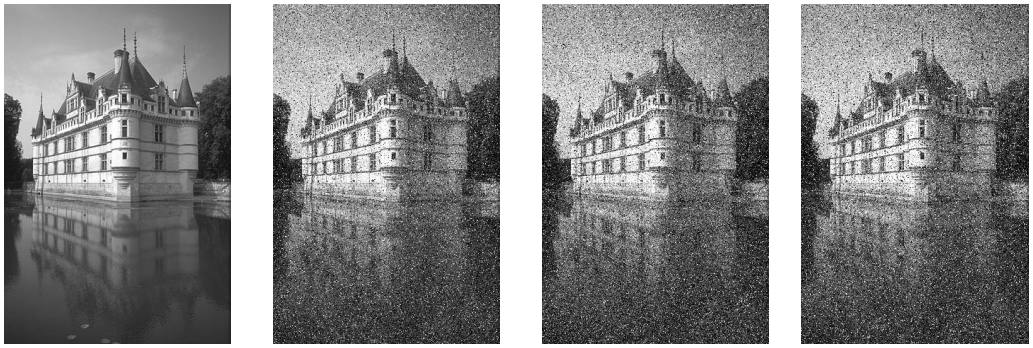

Original | f: $(\gamma, \sigma) = (10, 20)$ | $(\gamma, \sigma) = (10, 30)$ | $(\gamma, \sigma) = (15, 20)$

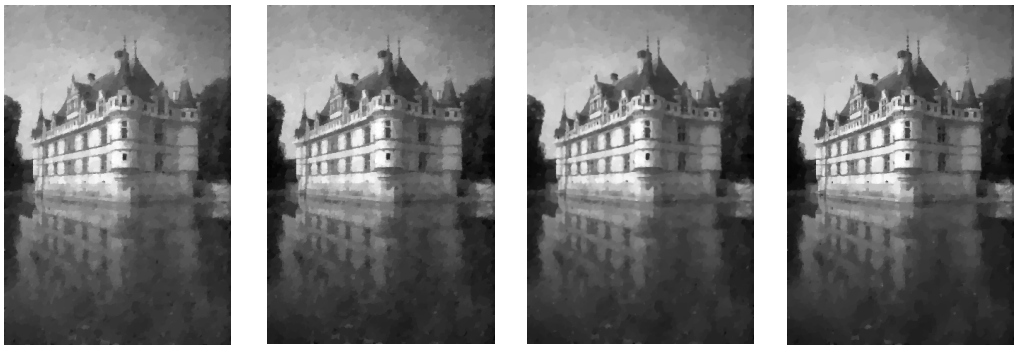

Cauchy-TV: 25.00 | L^1-TV: 25.11 | Yang et al.: 25.14 | Proposed: 25.84

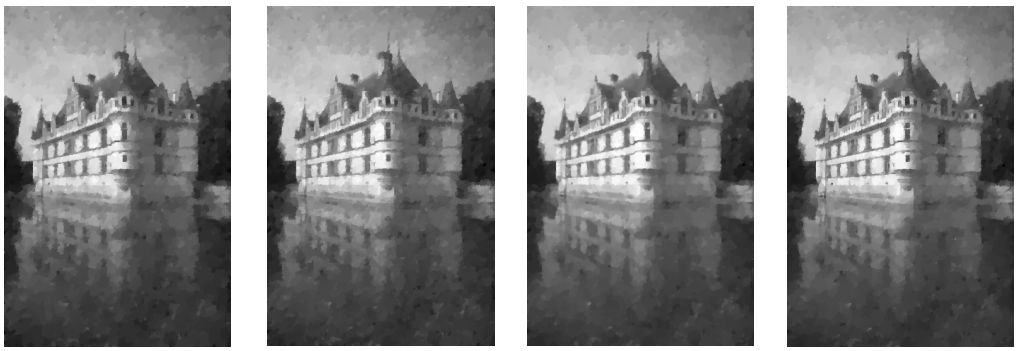

Cauchy-TV: 24.20 | L^1-TV: 24.56 | Yang et al.: 24.58 | Proposed: 24.97

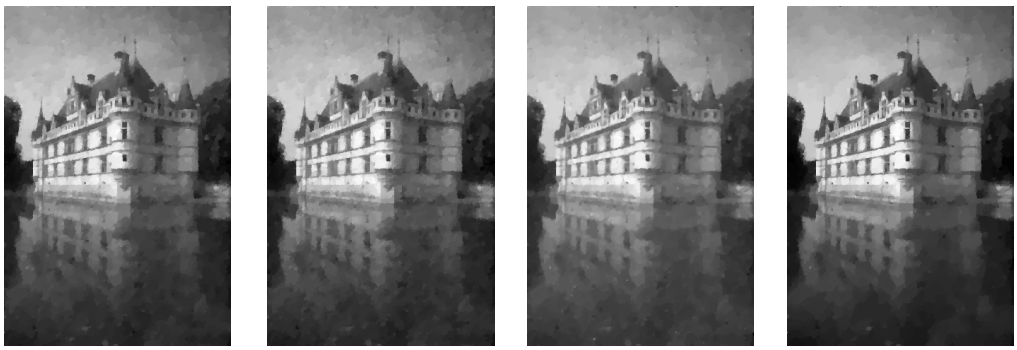

Cauchy-TV: 24.84 | L^1-TV: 24.71 | Yang et al.: 24.77 | Proposed: 25.17

Figure 10. Comparison of denoising results with different noise levels, $(\gamma, \sigma) = (10, 20)$ (2nd row), $(\gamma, \sigma) = (10, 30)$ (3rd row), $(\gamma, \sigma) = (15, 20)$ (4th row). Parameter λ_2 of the proposed model (top to bottom): 21, 20, 29.

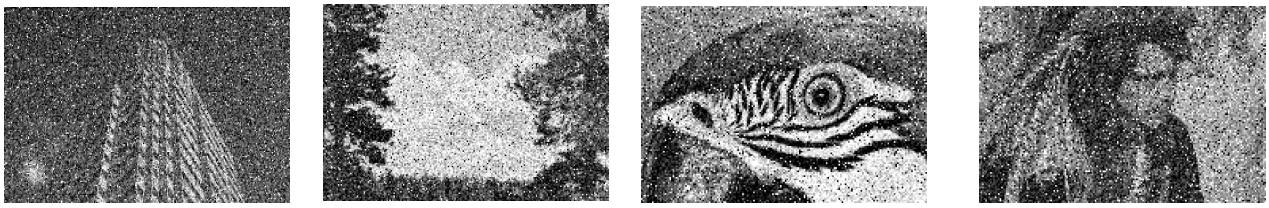

Zoomed noisy images when $(\gamma, \sigma) = (10, 30)$ (1st-2nd columns), $(\gamma, \sigma) = (15, 20)$ (3rd-4th columns)

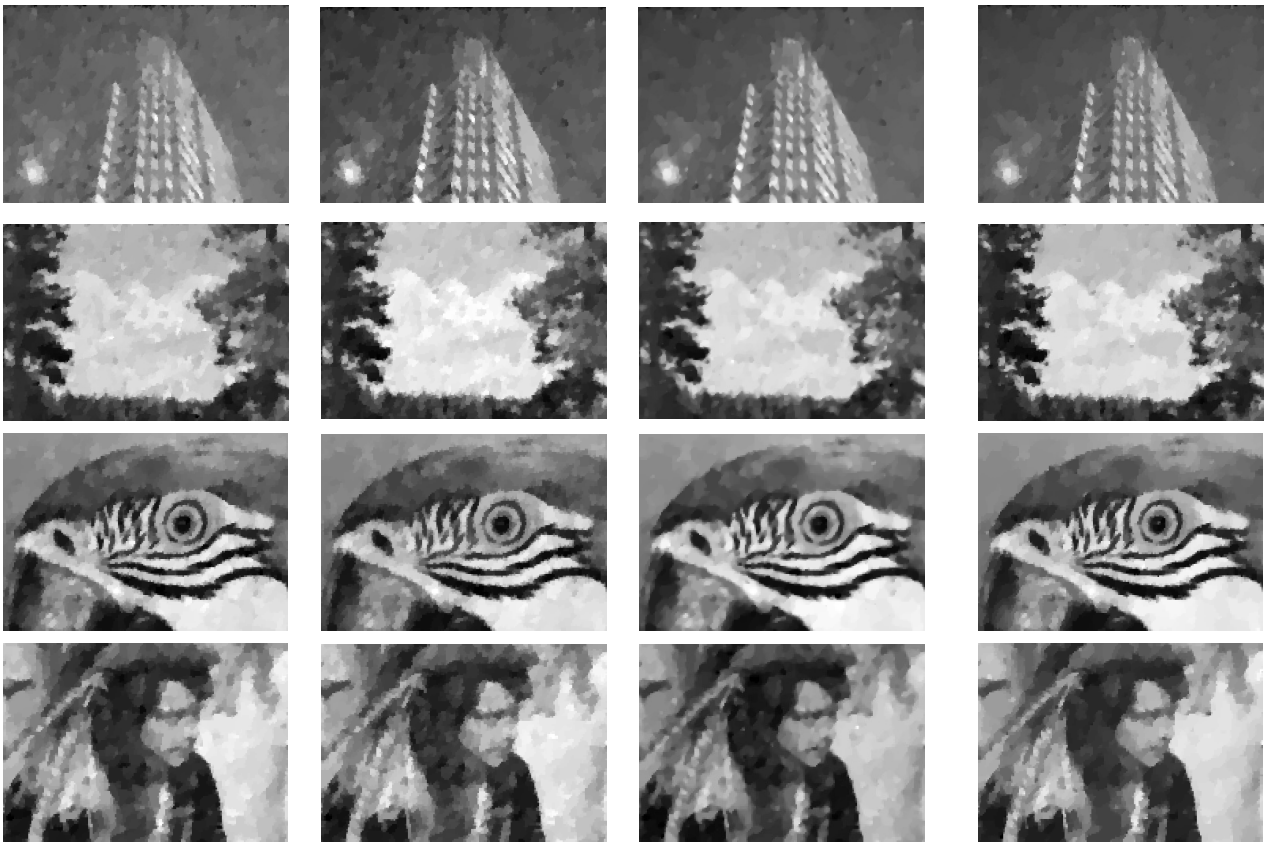

(a) Cauchy-TV [30] (b) L^1-TV [19] (c) Yang et al. [31] (d) Proposed

Figure 11. Zoomed denoised images using our model and other models when $(\gamma, \sigma) = (10, 30)$ (2nd-3rd rows), $(\gamma, \sigma) = (15, 20)$ (4th-5th rows). Parameter λ_2 of the proposed model (top to bottom): 20, 22, 31, 33.

Figure 12 presents the plots of the energy values $\mathcal{E}(u^k, v^k)$ in (3.4) and PSNR values of u^k via the outer iteration numbers k. In all cases, as the outer iteration increases, the energy values decrease and the PSNR values increase. Moreover, in Figure 13, we present the plots of relative errors of u and v. We can see that these relative errors generally decrease as the iteration increases, despite slight fluctuations in the relative errors of v. All of these illustrate the convergence behavior of the proposed iterative algorithm even though it is not theoretically proven.

In Figures 14 and 15, we compare the denoising results of the proposed model with different values for the parameter λ_2 in (3.2). In Figure 14, we present the denoising results when $(\gamma, \sigma) = (10, 20)$ and $(10, 30)$, while in Figure 15, we present the denoising resuls when $(\gamma, \sigma) = (10, 20)$ and $(15, 20)$. First, it can be observed that as λ_2 increases, the restored image u includes more details, but it also tends

to retain noise. Thus, we try to select a sufficiently denoised image with PSNR and SSIM values as high as possible for the best restored image. The optimal values of λ_2 may be different depending on images, as shown in the 1st rows in both figures, because different images have different structures and characteristics. Moreover, the optimal value of λ_2 depends on the noise level, as λ_2 is a regularization parameter that needs to be adjusted to obtain an adequately denoised image. Specifically, the optimal value of λ_2 tends to decrease as the Gaussian noise level σ increases, while it tends to increase as the Cauchy noise level γ increases, which can be seen in the 2nd rows in both figures. However, we note that the optimal values of λ_2 are restricted to some values; for all the test images except Bird, the optimal λ_2 is chosen from $\{21, 22, 23, 24\}$ when $(\gamma, \sigma) = (10, 20)$, $\{20, 21, 22, 23\}$ when $(\gamma, \sigma) = (10, 30)$ and $\{29, 30, 31, 32, 33, 34\}$ when $(\gamma, \sigma) = (15, 20)$, while λ_1 is fixed at 0.02. Furthermore, the restored images obtained by using the values in the same set do not change significantly and their PSNR and SSIM values change slightly, as shown in these examples. Hence, these examples show that the proposed model is not sensitive to the choice of parameter λ_2.

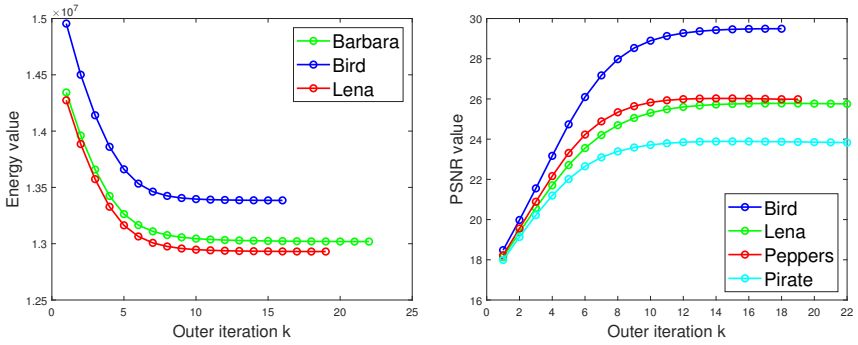

Figure 12. Plots of (left) energy values $\mathcal{E}(u^k, v^k)$ and (right) PSNR values of u^k via the outer iteration k, when (left) $(\gamma, \sigma) = (15, 10)$, (right) $(\gamma, \sigma) = (15, 20)$.

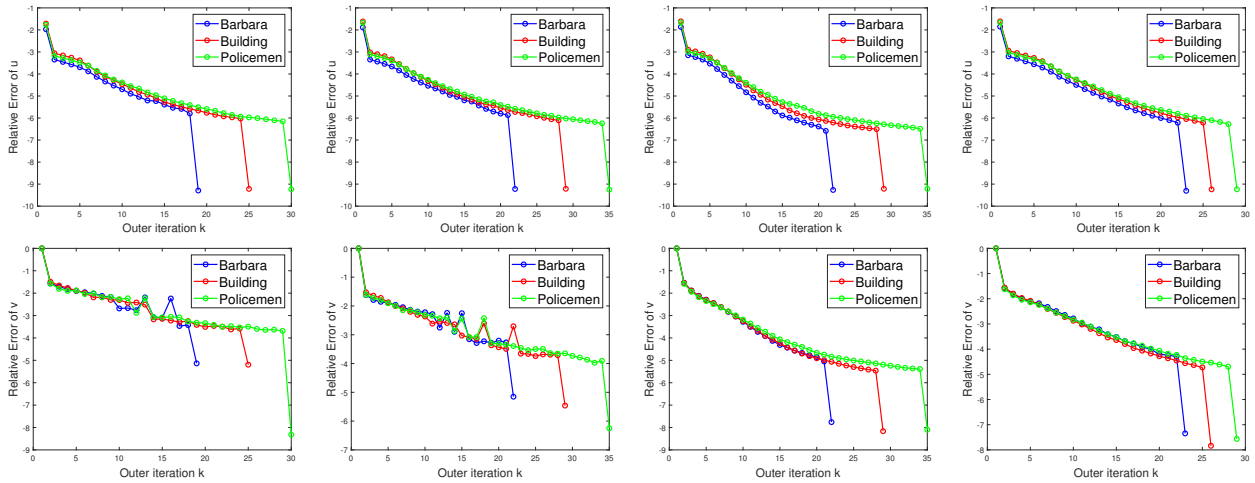

(a) $(\gamma, \sigma) = (10, 20)$ (b) $(\gamma, \sigma) = (10, 30)$ (c) $(\gamma, \sigma) = (15, 10)$ (d) $(\gamma, \sigma) = (15, 20)$

Figure 13. Plots of relative errors of u^k (top) and v^k (bottom) via the outer iteration k. Top: $\ln(\|u^{k+1} - u^k\|_2/\|u^{k+1}\|_2)$, bottom: $\ln(\|v^{k+1} - v^k\|_2/\|v^{k+1}\|_2)$.

(a) $\lambda_2 = 20$ 25.46/0.7804 | (b) $\lambda_2 = \mathbf{21}$ (best) **25.51/0.7811** | (c) $\lambda_2 = 22$ 25.58/0.7815 | (d) $\lambda_2 = 23$ 25.67/0.7789 | (e) $\lambda_2 = 24$ 25.70/0.7757

(a) $\lambda_2 = 19$ 24.38/0.7485 | (b) $\lambda_2 = \mathbf{20}$ (best) **24.55/0.7482** | (c) $\lambda_2 = 21$ 24.67/0.7459 | (d) $\lambda_2 = 22$ 24.71/0.7456 | (e) $\lambda_2 3$ 24.77/0.7401

Figure 14. Denoising results with different λ_2 in the proposed model, when $(\gamma, \sigma) = (10, 20)$ (top row), $(\gamma, \sigma) = (10, 30)$ (bottom row). PSNR/SSIM values are presented. *best* represents the optimal value of λ_2.

(a) $\lambda_2 = 20$ 24.15/0.5559 | (b) $\lambda_2 = 21$ 24.24/0.5624 | (c) $\lambda_2 = \mathbf{22}$ (best) **24.31/0.5690** | (d) $\lambda_2 = 23$ 24.37/0.5746 | (e) $\lambda_2 = 24$ 24.41/0.5796

(a) $\lambda_2 = 31$ 23.78/0.5382 | (b) $\lambda_2 = 32$ 23.82/0.5418 | (c) $\lambda_2 = \mathbf{33}$ (best) **23.83/0.5436** | (d) $\lambda_2 = 34$ 23.84/0.5466 | (e) $\lambda_2 = 35$ 23.85/0.5490

Figure 15. Denoising results with different λ_2 in the proposed model, when $(\gamma, \sigma) = (10, 20)$ (top row), $(\gamma, \sigma) = (15, 20)$ (bottom row). PSNR/SSIM values are presented. *best* represents the optimal value of λ_2.

Figure 16 presents the denoising results of the proposed model with two different values of λ_1 when $(\gamma, \sigma) = (15, 10)$. We recall that for the other noise cases such as $(\gamma, \sigma) = (10, 20)$, $(10, 30)$ and $(15, 20)$, λ_1 is fixed at 0.02. However, when $(\gamma, \sigma) = (15, 10)$, the restored images obtained with $\lambda_1 = 0.02$ tend to retain some Cauchy noise despite the parameter λ_2 being adjusted, as seen in the top row. This is due to that the Gaussian noise level is smaller than the other noise cases, which indicates that the parameter

λ_1 is influenced by the Gaussian noise level. By increasing the value of λ_1 to 0.05, we could obtain satisfactory restored images, as shown in the bottom row. We note that when $(\gamma, \sigma) = (15, 10)$, the optimal λ_2 is chosen from $\{27, 28, 29, 30, 31\}$ for all the test images. Thus, although the parameter λ_1 depends on the noise level, two values of λ_1 are enough to attain satisfactory denoising results. These imply that the choice of parameter λ_1 is not tricky in the proposed model.

In Figure 17, we present some denoising results of the proposed model with different values for the parameter γ in (3.2). Throughout the experiments, for the Yang's model and our model, the parameter γ is assumed to be the exact Cauchy noise level, denoted by γ_*. So we here present the denoising results when γ is not the accurate Cauchy noise level. Two values for γ are roughly chosen; one is smaller than γ_* while the other one is larger than γ_*. For the Lena image, we test with $\gamma = 5, 15$ when $\gamma_* = 10$, whereas for the Cameraman image, we test with $\gamma = 10, 20$ when $\gamma_* = 15$. It can be observed that even with the values for γ that are different from the precise noise level γ_*, we can attain similar denoising results to the ones obtained with γ_*, especially when $\gamma > \gamma_*$. These indicate that although $\gamma = \gamma_*$ generates the best denoising results, the parameter γ does not significantly affect the denoising results. The estimation for the parameter γ in the presence of mixed Cauchy-Gaussian noise is another effortful task, so we leave this problem as a future work.

(a) $\lambda_2 = 33$ 24.03/0.6154 | (b) $\lambda_2 = 34$ 24.10/0.6203 | (c) $\lambda_2 = 35$ 24.11/0.6212 | (d) $\lambda_2 = 36$ 24.13/0.6231 | (e) $\lambda_2 = 37$ 24.12/0.6228

(a) $\lambda_2 = 29$ 24.15/0.6335 | (b) $\lambda_2 = 30$ 24.30/0.6414 | (c) $\lambda_2 = \mathbf{31}$ (best) **24.42/0.6486** | (d) $\lambda_2 = 32$ 24.51/0.6539 | (e) $\lambda_2 = 33$ 24.59/0.6582

Figure 16. Denoising results with two different values of λ_1 in the proposed model, when $(\gamma, \sigma) = (15, 10)$. Top: $\lambda_1 = 0.02$, Bottom: $\lambda_1 = 0.05$. PSNR/SSIM values are presented. *best* represents the optimal value of λ_2.

(a) $\gamma = 5$: 26.36 (b) $\gamma = 10$: 26.45 (c) $\gamma = 15$: 26.37

(a) $\gamma = 10$: 25.14 (b) $\gamma = 15$: 25.28 (c) $\gamma = 20$: 25.35

Figure 17. Denoising results with different γ in the proposed model, when $(\gamma_*, \sigma) = (10, 20)$ (top row), $(\gamma_*, \sigma) = (15, 10)$ (bottom row). PSNR values are presented. Parameter λ_2 (left to right): (top) 9, 20, 31, (bottom) 22, 30, 38.

Lastly, in Table 5, the computational cost of the variational models is reported. The computational time of our model is the slowest among the models. Thus, there is a tradeoff between computing time and restoration performance. Despite the efficiency of our optimization algorithm, reducing the computational time of our model remains an issue.

Table 5. Computational time (in seconds) when $(\gamma, \sigma) = (10, 20)$.

Model/Image	Cauchy-TV [30]	L^1-TV [19]	Yang et al. [31]	Proposed
barbara	4.9	1.5	1.3	6.9
bird	8.6	3.2	2.0	10.8
boat	4.9	1.7	1.4	7.0
building	25.7	10.5	6.4	44.2
cameraman	4.6	2.4	1.6	7.2
castle	22.6	11.3	5.7	35.9
lake	4.9	1.8	1.7	6.5
lena	4.2	1.9	1.6	6.0
parrot	4.6	2.5	1.5	6.5
peppers	4.1	1.7	1.5	5.6
pirate	4.5	1.8	1.6	6.6
policemen	27.9	11.6	5.7	51.9

5. Conclusions

In this paper, we introduced a novel image denoising model under mixed Cauchy and Gaussian noise. The model is composed of a nonconvex data-fidelity term, expressed as an infimal convolution combination of two data-fidelity terms associated with two noise distributions, and total variation regularization. This new data-fidelity term enabled the separation of Cauchy noise and Gaussian noise

components. It facilitated simultaneous removal of both noise. Total variation regularization assisted in the sufficient elimination of the mixed noise in homogeneous regions, while keeping structural edges and fine features. Regardless of the nonconvexity of the model, we proved the existence of a minimizer. To solve the proposed model, we utilized an alternating minimization approach and the alternating direction method of multipliers. This contributed to an iterative algorithm, and its convergence was shown experimentally. Numerical results demonstrated the effectiveness of the proposed model, comparing to other existing models, regarding both visual aspect and image quality assessments. However, theoretical convergence analysis of the proposed algorithm remains an issue. Blind denoising with unknown Cauchy noise level γ is another demanding problem to be investigated in the future.

Acknowledgments

The author was supported by the Hankuk University of Foreign Studies Research Fund and the National Research Foundation of Korea (2021R1F1A1048111).

Conflict of interest

The authors declare no conflicts of interest in this paper.

References

1. M. Shinde, S. Gupta, Signal detection in the presence of atmospheric noise in tropics, *IEEE Trans. Commun.*, **22** (1974), 1055–1063. https://doi.org/10.1109/TCOM.1974.1092336
2. M. A. Chitre, J. R. Potter, S. H. Ong, Optimal and near optimal signal detection in snapping shrimp dominated ambient noise, *IEEE J. Oceanic Eng.*, **31** (2006), 497–503. https://doi.org/10.1109/JOE.2006.875272
3. S. Banerjee, M. Agrawal, Underwater acoustic communication in the presence of heavy-tailed impulsive noise with bi-parameter cauchy-gaussian mixture model, *2013 Ocean Electronics (SYMPOL)*, 2013, 1–7. https://doi.org/10.1109/SYMPOL.2013.6701903
4. G. A. Tsihrintzis, P. Tsakalides, C. L. Nikias, Signal detection in severely heavy-tailed radar clutter, *Conference Record of The Twenty-Ninth Asilomar Conference on Signals, Systems and Computers*, 1995, 865–869. https://doi.org/10.1109/ACSSC.1995.540823
5. E. E. Kuruoglu, W. J. Fitzgerald, P. J. W. Rayner, Near optimal detection of signals in impulsive noise modeled with asymmetric alpha-stable distribution, *IEEE Commun. Lett.*, **2** (1998), 282–284. https://doi.org/10.1109/4234.725224
6. H. El Ghannudi, L. Clavier, N. Azzaoui, F. Septier, P. A. Rolland, α-stable interference modeling and cauchy receiver for an ir-uwb ad hoc network, *IEEE Trans. Commun.*, **58** (2010), 1748–1757. https://doi.org/10.1109/TCOMM.2010.06.090074
7. M. Zimmermann, K. Dostert, Analysis and modeling of impulsive noise in broadband powerline communications, *IEEE Trans. Electromagn. Compat.*, **44** (2002), 249–258. https://doi.org/10.1109/15.990732

8. P. M. Reeves, *A non-gaussian turbulence simulation*, Air Force Flight Dynamics Laboratory, 1969.
9. A. Achim, P. Tsakalides, A. Bezerianos, Sar image denoising via bayesian wavelet shrinkage based on heavy-tailed modeling, *IEEE Trans. Geosci. Remote Sens.*, **41** (2003), 1773–1784. https://doi.org/10.1109/TGRS.2003.813488
10. Y. Peng, J. Chen, X. Xu, F. Pu, Sar images statistical modeling and classification based on the mixture of alpha-stable distributions, *Remote Sens.*, **5** (2013), 2145–2163. https://doi.org/10.3390/rs5052145
11. C. L. Nikias, M. Shao, *Signal processing with alpha-stable distri?butions and applications*, Hoboken, NJ, USA: Wiley, 1995.
12. S. A. Kassam, *Signal detection in non-gaussian noise*, *New York, USA: Springer*, 2012.
13. S. R. Krishna Vadali, P. Ray, S. Mula, P. K. Varshney, Linear detection of a weak signal in additive cauchy noise, *IEEE Trans. Commun.*, **65** (2017), 1061–1076. https://doi.org/10.1109/TCOMM.2016.2647599
14. J. Ilow, D. Hatzinakos, Detection in alpha-stable noise environments based on prediction, *Int. J. Adapt. Control Signal Proc.*, **11** (1997), 555–568.
15. D. Herranz, E. E. Kuruoglu, L. Toffolatti, An α-stable approach to the study of the p(d) distribution of unresolved point sources in cmb sky maps, *Astron. Astrophys.*, **424** (2004), 1081–1096. https://doi.org/10.1051/0004-6361:20035858
16. W. Feller, *An introduction to probability theory and its applications*, Vol. 2, 2 Eds., New York: John Wiley & Sons Inc., 1991.
17. N. L. Johnson, S. Kotz, N. Balakrishnan, *Continuous univariate distributions*, Vol. 1, 2 Eds., New York: Wiley, 1994.
18. L. Rudin, S. Osher, E. Fatemi, Nonlinear total variation based noise removal algorithm, *Phys. D*, **60** (1992), 259–268. https://doi.org/10.1016/0167-2789(92)90242-F
19. M. A. Nikolova, A variational approach to remove outliers and impulse noise, *J. Math. Imaging Vis.*, **20** (2004), 99–120. https://doi.org/10.1023/B:JMIV.0000011326.88682.e5
20. R. H. Chan, Y. Dong, M. Hintermuller, An efficient two-phase l1-tv method for restoring blurred images with impulse noise, *IEEE Trans. Image Process.*, **19** (2010), 1731–1739. https://doi.org/10.1109/TIP.2010.2045148
21. J. F. Cai, R. Chan, M. Nikolova, Fast two-phase image deblurring under impulse noise, *J. Math. Imaging Vis.*, **36** (2010), 46–53. https://doi.org/10.1007/s10851-009-0169-7
22. G. Aubert, J. F. Aujol, A variational approach to removing multiplicative noise, *SIAM J. Appl. Math.*, **68** (2008), 925–946. https://doi.org/10.1137/060671814
23. J. Shi, S. Osher, A nonlinear inverse scale space method for a convex multiplicative noise model, *SIAM J. Imaging Sci.*, **1** (2008), 294–321. https://doi.org/10.1137/070689954
24. Y. Dong, T. Zeng, A convex variational model for restoring blurred images with multiplicative noise, *SIAM J. Imaging Sci.*, **6** (2013), 1598–1625. https://doi.org/10.1137/120870621
25. J. Lu, L. Shen, C. Xu, Y. Xu, Multiplicative noise removal in imaging: An exp-model and its fixed-point proximity algorithm, *Appl. Comput. Harmon. Anal.*, **41** (2016), 518–539. https://doi.org/10.1016/j.acha.2015.10.003

26. T. Le, R. Chartrand, T. Asaki, A variational approach to reconstructing images corrupted by poisson noise, *J. Math. Imaging Vis.*, **27** (2007), 257–263. https://doi.org/10.1007/s10851-007-0652-y
27. P. Getreuer, M. Tong, L. A. Vese, A variational model for the restoration of mr images corrupted by blur and rician noise, In: *Advances in visual computing*, Lecture Notes in Computer Science, Berlin, Heidelberg: Springer, 2011. https://doi.org/10.1007/978-3-642-24028-7_63
28. L. Chen, T. Zeng, A convex variational model for restoring blurred images with large rician noise, *J. Math. Imaging Vis.*, **53** (2015), 92–111. https://doi.org/10.1007/s10851-014-0551-y
29. F. Sciacchitano, Y. Dong, T. Zeng, Variational approach for restoring blurred images with cauchy noise, *SIAM J. Imag. Sci.*, **8** (2015), 1894–1922. https://doi.org/10.1137/140997816
30. J. J. Mei, Y. Dong, T. Z. Hunag, W. Yin, Cauchy noise removal by nonconvex admm with convergence guarantees, *J. Sci. Comput.*, **74** (2018), 743–766. https://doi.org/10.1007/s10915-017-0460-5
31. Z. Yang, Z. Yang, G. Gui, A convex constraint variational method for restoring blurred images in the presence of alpha-stable noises, *Sensors*, **18** (2018). https://doi.org/10.3390/s18041175
32. Y. Chang, S. R. Kadaba, P. C. Doerschuk, S. B. Gelfand, Image restoration using recursive markov random field models driven by cauchy distributed noise, *IEEE Signal Process. Lett.*, **8** (2001), 65–66. https://doi.org/10.1109/97.905941
33. A. Achim, E. Kuruoğlu, Image denoising using bivariate α-stable distributions in the complex wavelet domain, *IEEE Signal Process. Lett.*, **12** (2005), 17–20. https://doi.org/10.1109/LSP.2004.839692
34. A. Loza, D. Bull, N. Canagarajah, A. Achim, Non-gaussian model-based fusion of noisy images in the wavelet domain, *Comput. Vis. Image Und.*, **114** (2010), 54–65.
35. Y. Wang, W. Yin, J. Zeng, Global convergence of ADMM in nonconvex nonsmooth optimization, *J. Sci. Comput.*, **78** (2019), 29–63. https://doi.org/10.1007/s10915-018-0757-z
36. J. Yang, Y. Zhang, W. Yin, An efficient TVL1 algorithm for deblurring multichannel images corrupted by impulsive noise, *SIAM J. Sci. Computing*, **31** (2009), 2842–2865. https://doi.org/10.1137/080732894
37. M. Ding, T. Z. Huang, S. Wang, J. J. Mei, X. L. Zhao, Total variation with overlapping group sparsity for deblurring images under cauchy noise, *Appl. Math. Comput.*, **341** (2019), 128–147. https://doi.org/10.1016/j.amc.2018.08.014
38. J. H. Yang, X. L. Zhao, J. J. Mei, S. Wang, T. H. Ma, T. Z. Huang, Total variation and high-order total variation adaptive model for restoring blurred images with cauchy noise, *Comput. Math. Appl.*, **77** (2019), 1255–1272. https://doi.org/10.1016/j.camwa.2018.11.003
39. G. Kim, J. Cho, M. Kang, Cauchy noise removal by weighted nuclear norm minimization, *J. Sci. Comput.*, **83** (2020), 1–21. https://doi.org/10.1007/s10915-020-01203-2
40. S. Lee, M. Kang, Group sparse representation for restoring blurred images with cauchy noise, *J. Sci. Comput.*, **83** (2020), 1–27. https://doi.org/10.1007/s10915-020-01227-8
41. M. Jung, M. Kang, Image restoration under cauchy noise with sparse representation prior and total generalized variation, *J. Comput. Math.*, **39** (2021), 81–107. https://doi.org/10.4208/jcm.1907-m2018-0234

42. L. Bai, A new approach for cauchy noise removal, *AIMS Math.*, **6** (2021), 10296–10312. https://doi.org/10.3934/math.2021596
43. X. Ai, G. Ni, T. Zeng, Nonconvex regularization for blurred images with cauchy noise, *Inverse Probl. Imag.*, **16** (2022), 625–646. https://doi.org/10.3934/ipi.2021065
44. J. F. Cai, R. H. Chan, M. Nikolova, Two-phase approach for deblurring images corrupted by impulse plus gaussian noise, *Inverse Probl. Imag.*, **2** (2008), 187–204. https://doi.org/10.3934/ipi.2008.2.187
45. Y. Xiao, T. Y. Zeng, J. Yu, M. K. Ng, Restoration of images corrupted by mixed gaussian-impulse noise via l_1-l_0 minimization, *Pattern Recogn.*, **44** (2010), 1708–1720. https://doi.org/10.1016/j.patcog.2011.02.002
46. R. Rojas P. Rodríguez, B. Wohlberg, Mixed gaussian-impulse noise image restoration via total variation, *2012 IEEE International Conference on Acoustics, Speech and Signal Processing (ICASSP)*, 2012, 1077–1080. https://doi.org/10.1109/ICASSP.2012.6288073
47. B. Dong, H. Ji, J. Li, Z. W. Shen, Y. H. Xu, Wavelet frame based blind image inpainting, *Appl. Comput. Harmon. Anal.*, **32** (2011), 268–279. https://doi.org/10.1016/j.acha.2011.06.001
48. J. Liu, X. C. Tai, H. Y. Huang, Z. D. Huan, A weighted dictionary learning models for denoising images corrupted by mixed noise, *IEEE Trans. Image Process.*, **22** (2013), 1108–1120. https://doi.org/10.1109/TIP.2012.2227766
49. M. Yan, Restoration of images corrupted by impulse noise and mixed gaussian impulse noise using blind inpainting, *SIAM J. Imaging Sci.*, **6** (2013), 1227–1245. https://doi.org/10.1137/12087178X
50. M. Hintermüller, A. Langer, Subspace correction methods for a class of nonsmooth and nonadditive convex variational problems with mixed L^1/L^2 data-fidelity in image processing, *SIAM J. Imaging Sci.*, **6** (2013), 2134–2173. https://doi.org/10.1137/120894130
51. A. Langer, Automated parameter selection in the L^1-L^2-TV model for removing Gaussian plus impulse noise, *Inverse Probl.*, **33** (2017). https://doi.org/10.1088/1361-6420/33/7/074002
52. A. Foi, M. Trimeche, V. Katkovnik, K. Egiazarian, Practical poissonian-gaussian noise modeling and fitting for single-image raw-data, *IEEE Trans. Image Process.*, **17** (2008), 1737–1754. https://doi.org/10.1109/TIP.2008.2001399
53. A. Jezierska, C. Chaux, J. Pesquet, H. Talbot, An EM approach for Poisson-Gaussian noise modeling, *2011 19th European Signal Processing Conference*, 2011, 2244–2248.
54. F. Murtagh, J. L. Starck, A. Bijaoui, Image restoration with noise suppression using a multiresolution support, *Astron. Astrophys. Suppl. Ser.*, **112** (1995), 179–189.
55. B. Begovic, V. Stankovic, L. Stankovic, Contrast enhancement and denoising of poisson and gaussian mixture noise for solar images, *2011 18th IEEE International Conference on Image Processing*, 2011, 185–188. https://doi.org/10.1109/ICIP.2011.6115829
56. F. Luisier, T. Blu, M. Unser, Image denoising in mixed Poisson-Gaussian noise, *IEEE Trans. Image Process.*, **20** (2011), 696–708. https://doi.org/10.1109/TIP.2010.2073477
57. M. Makitalo, A. Foi, Optimal inversion of the generalized anscombe transformation for Poisson-Gaussian noise, *IEEE Trans. Image Process.*, **22** (2013), 91–103. https://doi.org/10.1109/TIP.2012.2202675

58. Y. Marnissi, Y. Zheng, J. Pesquet, Fast variational bayesian signal recovery in the presence of Poisson-Gaussian noise, *2016 IEEE International Conference on Acoustics, Speech and Signal Processing (ICASSP)*, 2016, 3964–3968. https://doi.org/10.1109/ICASSP.2016.7472421

59. F. J. Anscombe, The transformation of poisson, binomial and negative-binomial data, *Biometrika*, **35** (1948), 246–254. https://doi.org/10.1093/biomet/35.3-4.246

60. F. Benvenuto, A. La Camera, C. Theys, A. Ferrari, H. Lantéri, M. Bertero, The study of an iterative method for the reconstruction of images corrupted by poisson and gaussian noise, *Inverse Probl.*, **24** (2008), 035016.

61. E. Chouzenoux, A. Jezierska, J. C. Pesquet, H. Talbot, A convex approach for image restoration with exact Poisson-Gaussian likelihood, *SIAM J. Imaging Sci.*, **8** (2015), 17–30. https://doi.org/10.1137/15M1014395

62. J. C. De los Reyes, C. B. Schönlieb, Image denoising: Learning the noise model via nonsmooth pde-constrained optimization, *Inverse Probl. Imaging*, **7** (2013), 1183–1214. https://doi.org/10.3934/ipi.2013.7.1183

63. L. Calatroni, C. Chung, J. C. De Los Reyes, C. B. Schönlieb, T. Valkonen, Bilevel approaches for learning of variational imaging models, In: *Variational methods: In imaging and geometric control*, Berlin, Boston: De Gruyter, 2017. https://doi.org/10.1515/9783110430394-008

64. D. N. H. Thanh, S. D. Dvoenko, A method of total variation to remove the mixed poisson-gaussian noise, *Pattern Recognit. Image Anal.*, **26** (2016), 285–293. https://doi.org/10.1134/S1054661816020231

65. L. Calatroni, J. C. De Los Reyes, C. B. Schönlieb, Infimal convolution of data discrepancies for mixed noise removal, *SIAM J. Imaging Sci.*, **10** (2017), 1196–1233. https://doi.org/10.1137/16M1101684

66. L. Calatroni, K. Papafitsoros, Analysis and automatic parameter selection of a variational model for mixed gaussian and salt-and-pepper noise removal, *Inverse Probl.*, **35** (2019), 114001.

67. J. Zhang, Y. Duan, Y. Lu, M. K. Ng, H. Chang, Bilinear constraint based admm for mixed poisson-gaussian noise removal, *SIAM J. Imaging Sci.*, **15** (2021), 339–366. https://doi.org/10.3934/ipi.2020071

68. Y. Chen, E. E. Kuruoglu, H. C. So, L. T. Huang, W. Q. Wang, Density parameter estimation for additive cauchy-gaussian mixture, *2014 IEEE Workshop on Statistical Signal Processing (SSP)*, 2014, 197–200. https://doi.org/10.1109/SSP.2014.6884609

69. Y. Chen, E. E. Kuruoglu, H. C. So, Optimum linear regression in additive cauchy-gaussian noise, *Signal Process.*, **106** (2015), 312–318. https://doi.org/10.1016/j.sigpro.2014.07.028

70. A. Chambolle, T. Pock, A first-order primal-dual algorithm for convex problems with applications to imaging, *J. Math. Imaging Vis.*, **40** (2011), 120–145. https://doi.org/10.1007/s10851-010-0251-1

71. F. Li, C. Shen, C. Shen J. Fan, Image restoration combining a total variational filter and a fourth-order filter, *J. Vis. Commun. Image Represent.*, **18** (2007), 322–330. https://doi.org/10.1016/j.jvcir.2007.04.005

72. K. Bredies, K. Kunisch, T. Pock, Total generalized variation, *SIAM J. Imaging Sci.*, **3** (2010), 492–526. https://doi.org/10.1137/090769521

73. G. Gilboa, S. Osher, Nonlocal operators with applications to image processing, *SIAM J. Multiscale Model. Simul.*, **7** (2009), 1005–1028. https://doi.org/10.1137/070698592

74. M. Aharon, M. Elad, A. Bruckstein, K-SVD: An algorithm for designing of overcomplete dictionaries for sparse representation, *IEEE Trans. Signal Process.*, **54** (2006), 4311–4322. https://doi.org/10.1109/TSP.2006.881199

75. M. Elad, M. Aharon, Image denoising via sparse and redundant representations over learned dictionaries, *IEEE Trans. Image Process.*, **15** (2006), 3736–3745. https://doi.org/10.1109/TIP.2006.881969

76. Y. R. Li, L. Shen, D. Q. Dai, B. W. Suter, Framelet algorithms for de-blurring images corrupted by impulse plus gaussian noise, *IEEE Trans. Image Process.*, **20** (2011), 1822–1837. https://doi.org/10.1109/TIP.2010.2103950

77. A. Chambolle, An algorithm for total variation minimization and applications, *J. Math. Imaging Vis.*, **20** (2004), 89–97. https://doi.org/10.1023/B:JMIV.0000011325.36760.1e

78. T. Goldstein, S. Osher, The split bregman method for L1-regularized problems, *SIAM J. Imaging Sci.*, **2** (2009), 323–343. https://doi.org/10.1137/080725891

79. S. Boyd, N. Parikh, E. Chu, B. Peleato, J. Eckstein, Distributed optimization and statistical learning via the alternating direction method of multipliers, *Found. Trends Mach. Learn.*, **3** (2010), 1–122. http://doi.org/10.1561/2200000016

80. C. Chen, M. K. Ng, X. L. Zhao, Alternating direction method of multipliers for nonlinear image restoration problems, *IEEE Trans. Image Process.*, **24** (2015), 33–43. http://doi.org/10.1109/TIP.2014.2369953

81. M. K. Ng, R. H. Chan, W. C. Tang, A fast algorithm for deblurring models with neumann boundary conditions, *SIAM J. Sci. Comput.*, **21** (1999), 851–866. https://doi.org/10.1137/S1064827598341384

82. N. Jacobson, *Basic algebra*, Freeman, New York, 1974.

83. B. R. Frieden, A new restoring algorithm for the preferential enhancement of edge gradients, *J. Opt. Soc. Am.*, **66** (1976), 280–283. https://doi.org/10.1364/JOSA.66.000280

84. J. P. Nolan, Numerical calculation of stable densities and distribution functions, *Commun. Stat. Stoch. Models*, **13** (1997), 759–774. https://doi.org/10.1080/15326349708807450

85. N. Balakrishnan, V. B. Nevzorov, *A primer on statistical distributions*, New York: John Wiley & Sons, 2003. https://doi.org/10.1002/0471722227

86. Z. Wang, A. C. Bovik, H. R. Sheikh, E. P. Simoncelli, Image quality assessment: From error visibility to structural similarity, *IEEE Trans. Image Process.*, **13** (2004), 600–612. https://doi.org/10.1109/TIP.2003.819861

Appendix A

For each fixed $x \in \Omega$, we define the function $h : \mathbb{R} \times \mathbb{R} \to \mathbb{R}$ as

$$h(s,t) = \lambda_1 t^2 + \lambda_2 \log(\gamma^2 + (s+t-f(x))^2) + \frac{\mu}{2}(s-g(x))^2.$$

The first-order and second-order partial derivatives of h are obtained as

$$\begin{aligned} &\frac{\partial h}{\partial s} = 2\lambda_2 \frac{s+t-f(x)}{\gamma^2 + (s+t-f(x))^2} + \mu(s-g(x)), \quad \frac{\partial h}{\partial t} = 2\lambda_2 \frac{s+t-f(x)}{\gamma^2 + (s+t-f(x))^2} + 2\lambda_1 t, \\ &\frac{\partial^2 h}{\partial s^2} = C + \mu, \quad \frac{\partial^2 h}{\partial t^2} = C + 2\lambda_1, \quad \frac{\partial^2 h}{\partial s \partial t} = C, \end{aligned} \tag{A.1}$$

where C is defined as

$$C = 2\lambda_2 \frac{\gamma^2 - (s+t-f(x))^2}{(\gamma^2 + (s+t-f(x))^2)^2}.$$

It can be easily proven that if $4\gamma^2\mu \geq \lambda_2$, then $\frac{\partial^2 h}{\partial s^2}(s,\cdot) \geq 0$, so h is convex with respect to the variable s. Then, $\frac{\partial h}{\partial s}(s,\cdot) = 0$ is equivalent to a cubic equation that has either two real roots or one real root. Thus, the function $h(s,\cdot)$ has only one minimizer, so $h(s,\cdot)$ is strictly convex if $4\gamma^2\mu \geq \lambda_2$. Similarly, if $8\gamma^2\lambda_1 \geq \lambda_2$, then $\frac{\partial^2 h}{\partial t^2}(\cdot,t) \geq 0$, so h is strictly convex with respect to t. Moreover, for the convexity of h on $\mathbb{R} \times \mathbb{R}$, the Hessian matrix of h needs to be positive semi-definite. That is, in addition to the aforementioned constraints, the determinant of the Hessian matrix of h should be nonnegative:

$$\frac{\partial^2 h}{\partial s^2}\frac{\partial^2 h}{\partial t^2} - \Big(\frac{\partial^2 h}{\partial s \partial t}\Big)^2 = C(\mu + 2\lambda_1) + 2\mu\lambda_1 \geq 0.$$

This inequality holds if $\lambda_2(\mu + 2\lambda_1) \leq 8\gamma^2\mu\lambda_1$, which is satisfied when $\lambda_2 \leq \frac{1}{2}\min\{8\gamma^2\lambda_1, 4\gamma^2\mu\}$. Thus, if $\lambda_2 \leq \frac{1}{2}\min\{8\gamma^2\lambda_1, 4\gamma^2\mu\}$, then the Hessian matrix of h is positive semi-definte, so h is convex. In addition, h is strictly convex if $\lambda_2 < \frac{1}{2}\min\{8\gamma^2\lambda_1, 4\gamma^2\mu\}$.